Article

Current Biology

Aberrant Tonic Inhibition of Dopaminergic Neuronal Activity Causes Motor Symptoms in Animal Models of Parkinson's Disease

Graphical Abstract

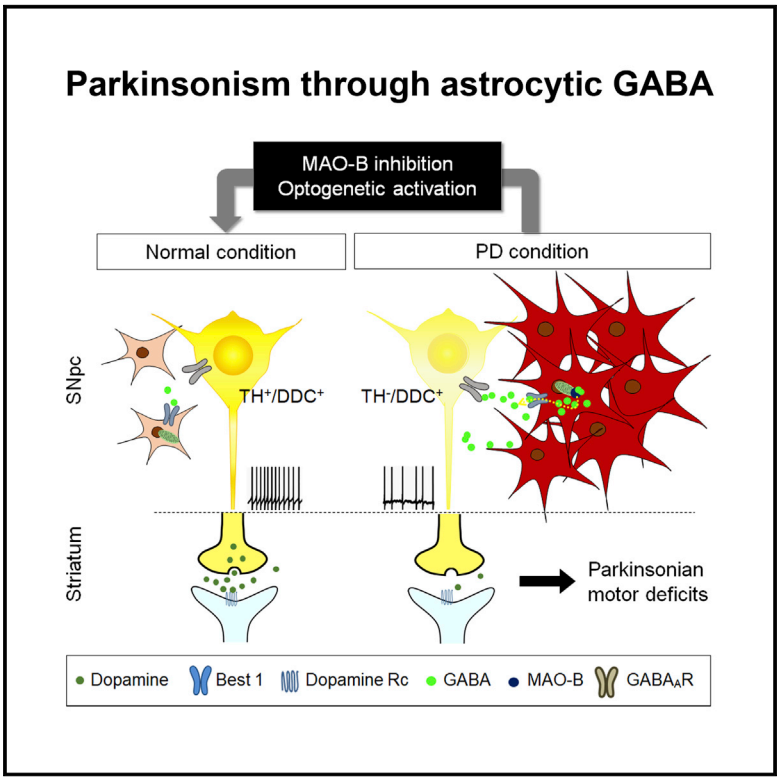

Highlights

- Reactive astrocytes in SNpc produce excessive GABA via MAO-B in animal models of PD
- Aberrant tonic inhibition causes reduced DA production in neurons and motor deficits
- Dormant neurons are rescued by MAO-B inhibition or optogenetic neuronal activation

Authors

Jun Young Heo, Min-Ho Nam, Hyung Ho Yoon, ..., Hoon Ryu, Sang Ryong Jeon, C. Justin Lee

Correspondence

hoonryu@bu.edu (H.R.), srjeon@amc.seoul.kr (S.R.J.), cjl@ibs.re.kr (C.J.L.)

In Brief

Heo et al. report that astrocytic GABA-mediated aberrant tonic inhibition of DA neurons leads to a reduction in TH expression and dopamine production, causing dormant DA neurons and motor deficits. Blocking astrocytic GABA synthesis by MAO-B inhibition or optogenetic activation of dormant DA neurons reverses PD pathology.

Heo et al., 2020, Current Biology *30*, 276–291
January 20, 2020
https://doi.org/10.1016/j.cub.2019.11.079

CellPress

CellPress

Current Biology
Article

Aberrant Tonic Inhibition of Dopaminergic Neuronal Activity Causes Motor Symptoms in Animal Models of Parkinson's Disease

Jun Young Heo,[1,2,3,25] Min-Ho Nam,[1,4,25] Hyung Ho Yoon,[5,25] Jeongyeon Kim,[1,6,25] Yu Jin Hwang,[7,25] Woojin Won,[1,8] Dong Ho Woo,[1] Ji Ae Lee,[9] Hyun-Jung Park,[4] Seonmi Jo,[1,10,11] Min Joung Lee,[2,3] Sunpil Kim,[1,8] Jeong-Eun Shim,[12] Dong-Pyo Jang,[12] Kyoung I. Kim,[13] Sue H. Huh,[13] Jae Y. Jeong,[13] Neil W. Kowall,[14,15,16] Junghee Lee,[14,15,16] Hyeonjoo Im,[1,7] Jong Hyun Park,[17] Bo Ko Jang,[17] Ki Duk Park,[17] Hyunjoo J. Lee,[18] Hyogeun Shin,[18] Il-Joo Cho,[18] Eun Mi Hwang,[23] YoungSoo Kim,[7,19] Hye Yun Kim,[19] Soo-Jin Oh,[1,17] Seung Eun Lee,[24] Sun Ha Paek,[20] Jong Hyuk Yoon,[21] Byung K. Jin,[13] Gi Ryang Kweon,[2,3] Insop Shim,[4] Onyou Hwang,[9] Hoon Ryu,[1,7,14,15,16,*] Sang Ryong Jeon,[5,*] and C. Justin Lee[1,8,22,26,*]

[1]Center for Neuroscience, Korea Institute of Science and Technology (KIST), Seoul 02792, Korea
[2]Department of Medical Science, College of Medicine, Chungnam National University, Daejeon 35015, Korea
[3]Infection Control Convergence Research Center, College of Medicine, Chungnam National University, Daejeon 35015, Korea
[4]Department of Science in Korean Medicine, Graduate School, Kyung Hee University, Seoul 02447, Korea
[5]Department of Neurological Surgery, Asan Medical Center, University of Ulsan College of Medicine, Seoul 05505, Korea
[6]Emotion, Cognition and Behavior Research Group, Korea Brain Research Institute, Daegu 41062, Korea
[7]Center for Neuro-Medicine, Brain Science Institute, KIST, Seoul 02792, Korea
[8]KU-KIST Graduate School of Converging Science of Technology, Korea University, Seoul 02841, Korea
[9]Department of Biochemistry and Molecular Biology, University of Ulsan College of Medicine, Seoul 05505, Korea
[10]Department of Biological Sciences, Korea Advanced Institute of Science and Technology (KAIST), Daejeon 34141, Korea
[11]Department of Genetic Resources Research, National Marine Biodiversity Institute of Korea, Seocheon 33662, Korea
[12]Department of Biomedical Engineering, Hanyang University, Seoul 04763, Korea
[13]Department of Biochemistry & Molecular Biology, Department of Neuroscience, Neurodegeneration Control Research Center, School of Medicine, Kyung Hee University, Seoul 02447, Korea
[14]Boston University Alzheimer's Disease Center, Boston University School of Medicine, Boston, MA 02118, USA
[15]Department of Neurology, Boston University School of Medicine, Boston, MA 02118, USA
[16]VA Boston Healthcare System, Boston, MA 02132, USA
[17]Convergence Research Center for Dementia, KIST, Seoul 02792, Korea
[18]Center for BioMicrosystems, Brain Science Institute, KIST, Seoul 02792, Korea
[19]Department of Pharmacy, Yonsei Institute of Pharmaceutical Sciences, and Integrated Science and Engineering Division, Yonsei University, Incheon 21983, Korea
[20]Department of Neurosurgery, Seoul National University Hospital, Seoul 03080, Korea
[21]Neurodegenerative Diseases Research Group, Korea Brain Research Institute, Daegu 41062, Korea
[22]Center for Cognition and Sociality, Institute for Basic Science, Daejeon 34126, Korea
[23]Center for Functional Connectomics, KIST, Seoul 02792, Korea
[24]Virus Facility, Research Animal Resource Center, KIST, Seoul 02792, Korea
[25]These authors contributed equally
[26]Lead Contact
*Correspondence: hoonryu@bu.edu (H.R.), srjeon@amc.seoul.kr (S.R.J.), cjl@ibs.re.kr (C.J.L.)
https://doi.org/10.1016/j.cub.2019.11.079

SUMMARY

Current pharmacological treatments for Parkinson's disease (PD) are focused on symptomatic relief, but not on disease modification, based on the strong belief that PD is caused by irreversible dopaminergic neuronal death. Thus, the concept of the presence of dormant dopaminergic neurons and its possibility as the disease-modifying therapeutic target against PD have not been explored. Here we show that optogenetic activation of substantia nigra pars compacta (SNpc) neurons alleviates parkinsonism in acute PD animal models by recovering tyrosine hydroxylase (TH) from the TH-negative dormant dopaminergic neurons, some of which still express DOPA decarboxylase (DDC). The TH loss depends on reduced dopaminergic neuronal firing under aberrant tonic inhibition, which is attributed to excessive astrocytic GABA. Blocking the astrocytic GABA synthesis recapitulates the therapeutic effect of optogenetic activation. Consistently, SNpc of postmortem PD patients shows a significant population of TH-negative/DDC-positive dormant neurons surrounded by numerous GABA-positive astrocytes. We propose that disinhibiting dormant dopaminergic neurons by blocking excessive astrocytic GABA could be an effective therapeutic strategy against PD.

INTRODUCTION

The motor symptoms of Parkinson's disease (PD) are mostly attributed to irreversible dopamine depletion, which is believed

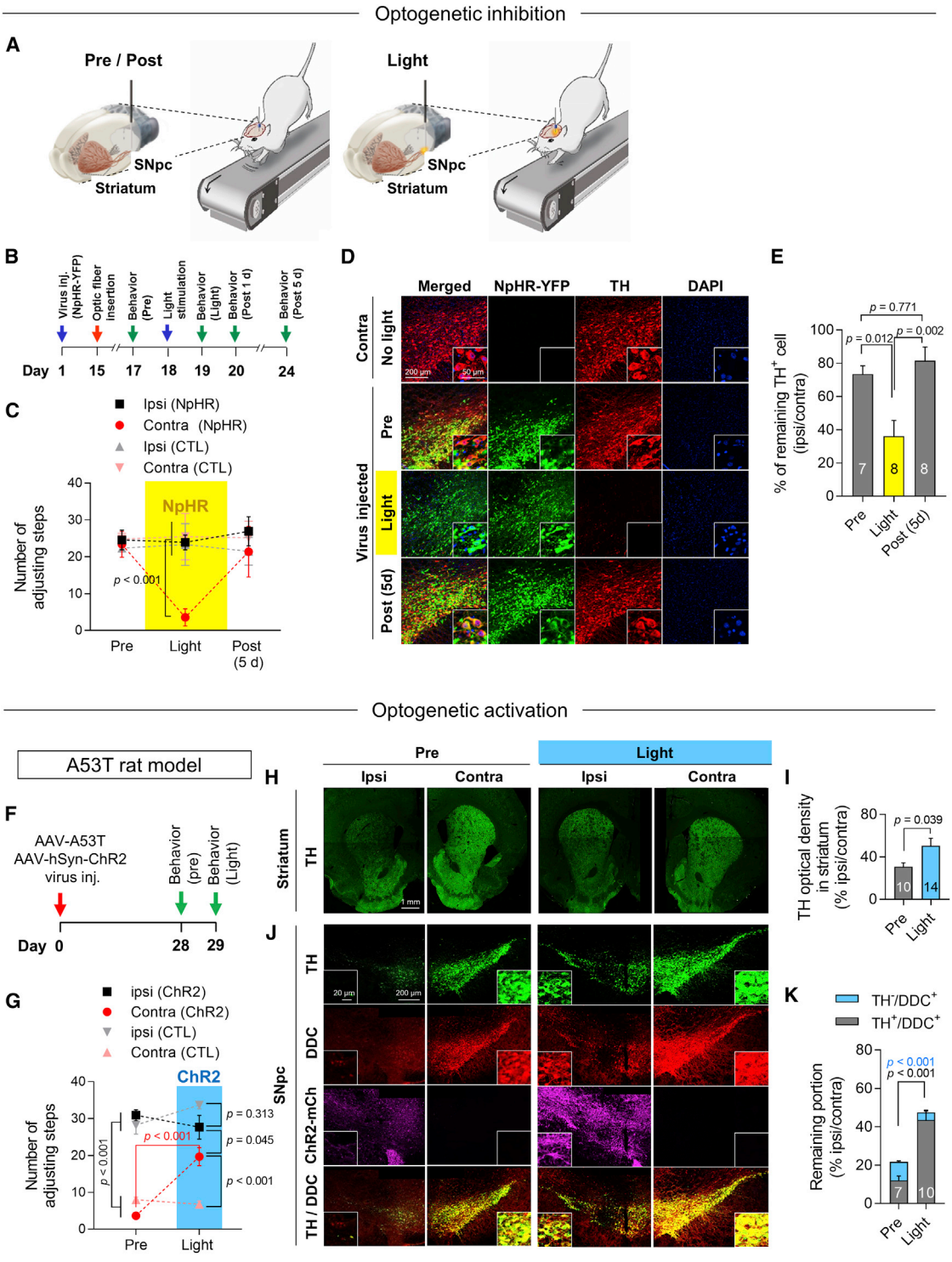

Figure 1. Optogenetic Modulation Bi-directionally Regulates TH and Parkinsonian Motor Symptoms

(A) Schematic diagram of optogenetic inhibition and stepping test.

(B) Experimental protocol of optogenetic inhibition of DA neurons in SNpc of naive rats.

(C) Number of adjusting steps during optogenetic inhibition (yellow) (N = 6 for NpHR and N = 3 for control).

(D) Representative confocal images of TH in SNpc with NpHR-YFP expression.

(E) Portions of remaining TH^+ neurons in ipsilateral SNpc compared to contralateral SNpc (N = 4 for each condition).

(F) Experimental protocol of optogenetic activation of DA neurons in SNpc of A53T rat models.

(G) Number of adjusting steps during optogenetic activation (blue) (N = 5 for ChR2 and N = 6 for control).

(legend continued on next page)

to be caused by an extensive loss of dopaminergic (DA) neurons in the substantia nigra pars compacta (SNpc) [1]. However, these motor symptoms can be reversible under certain pathological conditions referred to as parkinsonism, which includes chronic use of valproate [2], vitamin B12 deficiency [3], asymptomatic hypopituitarism [4], and Epstein-Barr virus encephalitis [5]. These reports imply that dopamine depletion can be reversible and caused by mechanisms other than DA neuronal loss.

The reversibility of dopamine depletion may be explained by the fact that expression of tyrosine hydroxylase (TH), the key dopamine-producing enzyme, can be regulated by neuronal activity [6–8]. Optogenetic modulation of DA neuronal activity has been recently reported to bidirectionally modulate TH expression and motor function in *Drosophila* [9]. In addition, reduced DAT expression [10], reduced VMAT2 expression [11], and synaptic terminal loss and axonal damage [12] are known to precede DA neuronal death. Therefore, it is plausible that live DA neurons in SNpc lose their TH level and become dormant, when the DA neuronal activity is suppressed. However, the existence of dormant DA neurons in SNpc of rodent models and PD patients has not been demonstrated. Furthermore, a possibility of restoring the activity of the dormant DA neurons to rescue TH expression and dopamine production as a therapeutic strategy against PD has not been tested.

In recent years, glial cells have received special attention as their activation contributes to neuroinflammation including reactive astrocytosis, which has been implicated in the progression of PD [13–17]. The reactive astrocytes have traditionally been considered a byproduct of neurodegeneration [18]. However, reactive astrocytes can be the origin of neuronal dysfunction and degeneration in a non-cell-autonomous fashion [16, 19–21]. In addition, genetic mutations associated with PD, such as overexpression of α-synuclein [22, 23] and loss of PINK1 [24] or DJ-1 [25], have been reported to cause astrogliosis prior to neuronal loss [24]. In toxin-induced PD animal models, such as the MPTP model, glial activation precedes the loss of TH-positive neurons [26]. However, whether and how astrocytic reactiveness can lead to DA neuronal dysfunction in etiology of PD has not yet been thoroughly investigated.

We have recently demonstrated that astrocytes synthesize and release the major inhibitory transmitter GABA through monoamine oxidase-B (MAO-B) and the Best1 channel, respectively, especially when they become reactive under pathological conditions [27–30]. The presence of extensive reactive astrocytes in the SNpc of PD patients alludes to the involvement of augmented astrocytic GABA. Moreover, early intervention of irreversible MAO-B inhibitors such as selegiline and rasagiline is reported to be efficacious for lowering the daily dose of levodopa [31], although their potential effect on improving motor symptoms of the late-stage PD patients is controversial. These raise a possibility that GABA from reactive astrocytes might participate in the early stage of PD through downregulating DA neuronal activity. To test this hypothesis, we investigate and demonstrate that suppressed neuronal activity causes TH loss and parkinsonian motor symptoms, which can be alleviated by blocking excessive astrocytic GABA synthesis, with acute genetic and sporadic PD animal models. Given these findings, we suggest that reactivation of dormant DA neurons by blocking excessive tonic inhibition mediated by astrocytic GABA could be a possible therapeutic strategy for the early-stage PD patients.

RESULTS

Optogenetic Inhibition of SNpc Neurons Induces Parkinsonian Motor Symptoms

We investigated if transient optogenetic inhibition of SNpc neurons can cause long-lasting TH loss and parkinsonian motor deficits. To optogenetically inhibit SNpc neuronal firing including DA firing, naive rats received unilateral injections of adeno-associated virus (AAV) containing halorhodopsin (*Natronomonas pharaonis*) under the human synapsin-1 promoter (AAV-hSynapsin1-NpHR-YFP). This NpHR was preferentially expressed in DA neurons (Figures S1A and S1B). We evaluated the motor function with a stepping test and performed immunohistochemistry to assess the level of TH expression in the same rats. After a 24 h period of light stimulation (590 nm, 100 ms, 5 Hz) [32], the contralateral forepaw showed a deficit of adjusting steps, which was completely recovered by a 5-day rest without light stimulation (Figures 1A–1C). Notably, after light stimulation had been stopped, the rats continued to show severe motor impairments after 1 day (Figure S1C), and it took several days to recover fully (Figure 1C). The same laser stimulation without opsin expression failed to induce behavioral recovery (Figure 1C). We confirmed the functionality of the expressed NpHR-YFP by *ex vivo* and *in vivo* electrophysiology (Figures S1D–S1F) and immunohistochemistry (Figure 1D). In accordance with the impaired motor symptoms upon light stimulation, we found a significant decrease in the ratio of remaining TH-positive (TH^+) neurons in the ipsilateral SNpc to that in the contralateral SNpc. The decreased portion of remaining TH^+ neurons was completely recovered by a 5-day rest without light stimulation (Figures 1D and 1E). These results suggest that direct inhibition of SNpc neuronal firing causes a long-lasting reduction in TH expression, leading to parkinsonian motor symptoms with no distinct neuronal loss.

Optogenetic Activation of SNpc Neurons Alleviates Parkinsonian Motor Symptoms

Next, we asked whether optogenetic activation of SNpc neurons including DA neurons can restore TH expression and motor symptoms in already established acute PD models. To test this possibility, we utilized two different acute PD animal models: a rat PD model of viral overexpression of A53T α-synuclein [33, 34] (A53T rat model) and a 6-hydroxydopamine (6-OHDA) rat PD model [35]. We first verified the A53T rat model as an acute

(H) Representative confocal images of TH in striatum.
(I) TH optical density in striatum before and after optogenetic activation (N = 3 and 4 for respective condition).
(J) Representative confocal images of TH and DDC in SNpc with ChR2-YFP expression.
(K) Portions of remaining TH^+ and DDC^+ neurons in ipsilateral SNpc compared to contralateral SNpc (N = 3 and 4 for respective condition). Numbers on each bar refer to the numbers of slices.
For all panels, mean ± SEM. Additional statistical details are provided in Table S2. See also Figure S1.

genetic model induces a substantial decrease of nigrostriatal TH and impaired stepping behaviors within 3 weeks (Figures 1G–1K). For optogenetic stimulation, we unilaterally delivered AAV containing Channelrhodopsin-2 (AAV-hSynapsin1-ChR2-YFP) to neurons in the SNpc of the A53T rat model (Figures 1F, S1G, and S1H). Intriguingly, 24 h light stimulation (470 nm, 6 ms, 5 Hz) [36] given to freely moving rats significantly recovered from the α-synuclein-induced stepping dysfunction of the contralateral forepaw (Figure 1G). The same laser stimulation without opsin expression did not induce behavioral recovery (Figure 1G). Optogenetic activation was confirmed by *ex vivo* and *in vivo* electrophysiology (Figures S1J–S1L). In accordance with the motor recovery, we found a significant increase in optical density of striatal TH after ChR2 activation in the A53T rat model (Figures 1H and 1I). This could be attributed to either increase of TH protein level in the finite number of remaining DA neurons or increase of the number of remaining TH^+ neurons in the ipsilateral SNpc. We found that the light stimulation significantly increased the ratio of remaining TH^+ neurons in the ipsilateral SNpc to that in the contralateral SNpc (Figures 1J and 1K). This finding implies that the increased level of striatal TH is more likely derived from the substantial increase in the number of TH^+ neurons in the SNpc. We recapitulated the recovery effect of optogenetic activation of SNpc neurons in another well-established PD model, the 6-OHDA rat model (Figures S1M–S1Q).

The results from optogenetic experiments raise a possibility that a significant population of rescuable TH-negative (TH^-) neurons, whose TH expression had been downregulated by suppressed neuronal activity, is present in the SNpc of A53T and 6-OHDA rat models. To test this possibility, we investigated the expression pattern of DOPA decarboxylase (DDC), another essential enzyme for dopamine synthesis (Figure S1R). We found a significant population of TH^- but DDC-positive (TH^-/DDC^+) neurons in the SNpc of the A53T rat model prior to optogenetic activation (Figures 1J and 1K). These TH^-/DDC^+ neurons represent surviving dormant DA neurons that cannot produce dopamine due to the lack of TH. In addition to TH^+ neurons, we found that the number of DDC^+ neurons was increased by optogenetic activation (Figure 1K), implying that there is a substantial number of TH^- and DDC-negative (TH^-/DDC^-) surviving dormant DA neurons that could be rescued. Taken together, these findings suggested that suppressing or activating the SNpc neuronal activity is sufficient to cause or alleviate parkinsonian motor symptoms, respectively.

Dormant TH^-/DDC^+ Neurons in SNpc of PD Animal Models

To investigate the existence of the dormant TH^-/DDC^+ neurons in acute PD animal models, we utilized three different animal models of PD including the A53T mouse model (Figures 2A, S2A, and S2B) as an acute genetic model and two different toxin-based models: the 6-OHDA (6-hydroxydopamine) rat model (Figure 2F), mimicking the extensive loss of DA neurons in PD (>90%) [35], and the MPTP (1-methyl-4-phenyl-1,2,3,6-tetrahydropyridine) mouse model (Figure 2K), mimicking the early stage and mild state of PD with 60%–70% of SNpc DA neuronal loss [37]. We performed immunohistochemistry with antibodies against TH and DDC to identify the population of TH^-/DDC^+ neurons. We found that the number of SNpc TH^+ neurons was significantly decreased in the entire A53T mouse model (Figures 2B and 2C), 6-OHDA rat model (Figures 2G, 2H, and S2D), and MPTP mouse model (Figures 2L and 2M). In addition, the numbers of SNpc DDC^+ neurons were decreased in the A53T and 6-OHDA models (Figures 2D and 2I), but not in the MPTP mouse model (Figure 2N). Notably, the stereological assessment showed that the number of TH^+ neurons in the ipsilateral SNpc was decreased by ~71% (from 3,900 to 1,135) while the number of DDC^+ neurons was only decreased by ~54% (from 4,277 to 1,978) (Figures 2C and 2D). Moreover, we found 25.5% of TH^-/DDC^+ neurons among total DDC^+ neurons in the ipsilateral SNpc of the A53T-overexpressed mice (Figures 2E and S2C). In the 6-OHDA model, the remaining portion of ipsilateral DDC^+ neurons was significantly greater than that of ipsilateral TH^+ neurons (Figure 2J), indicating that TH expression is more susceptible to the PD-related insults than that of DDC. In the MPTP mouse model, we also detected 46.72% of TH^-/DDC^+ neurons among total DDC^+ SNpc neurons (Figure 2O). These neurons were confirmed to be alive by 1 week as evidenced by the absence of propidium iodide (PI) staining (Figures S2E and S2F), but eventually degenerated after 3 weeks (Figures S2G–S2I). This neuronal death observed 3 weeks after MPTP administration was associated with reactive oxygen species, which might be generated from MAO-B's action (Figures S2J–S2L). The surviving DDC^+ neurons from the insults such as A53T α-synuclein overexpression, 6-OHDA, or MPTP showed decreased soma sizes (Figure S2M), indicating that the neurons are atrophied and possibly undergoing neurodegeneration. These findings raise a possibility that the dormant, incapable of producing dopamine, but still surviving DA neurons can be reactivated by eliciting neuronal activity.

Restoration of TH in Dormant Neurons by MAO-B Inhibition in PD Models

We next asked if MAO-B inhibition can restore the TH level of the dormant TH^-/DDC^+ neurons in the SNpc. MAO-B inhibitors are prescribed to PD patients as an adjuvant therapy to levodopa treatment, and their mode of action has been believed to prevent dopamine breakdown. We found that A53T α-synuclein-overexpressed MAO-B knockout (KO) mice [38] were relatively resistant to α-synuclein-induced TH loss in SNpc, compared to WT mice (Figures 2C, S2N, and S2O). Next, we tested if oral treatment of selegiline, one of the most widely used irreversible MAO-B inhibitors, can reverse the TH loss in MPTP and 6-OHDA models. Selegiline treatment (3 days post-treatment; Figure 2K) significantly recovered the number of SNpc TH^+ neurons and striatal TH levels in the MPTP model (Figures 2M, S2P, and S2Q). Compared to the MPTP model, the 6-OHDA model is a more severe model of PD that requires relatively long-term therapy. Based on our recent finding that long-term treatment of selegiline causes irreversible breakdown of MAO-B and turns on an undesirable compensatory mechanism [39], we treated the 6-OHDA animals with safinamide (a 2-week regimen; Figure 2F), a reversible MAO-B inhibitor that improves several critical drawbacks of irreversible MAO-B inhibitors such as selegiline [39]. We found that safinamide treatment caused a significant recovery of the numbers of TH^+ and DDC^+ neurons in the SNpc of the 6-OHDA model (Figure 2H). However, this estimation and calculations of percentages of cells were based on sampling from a limited number of brain sections and taking the

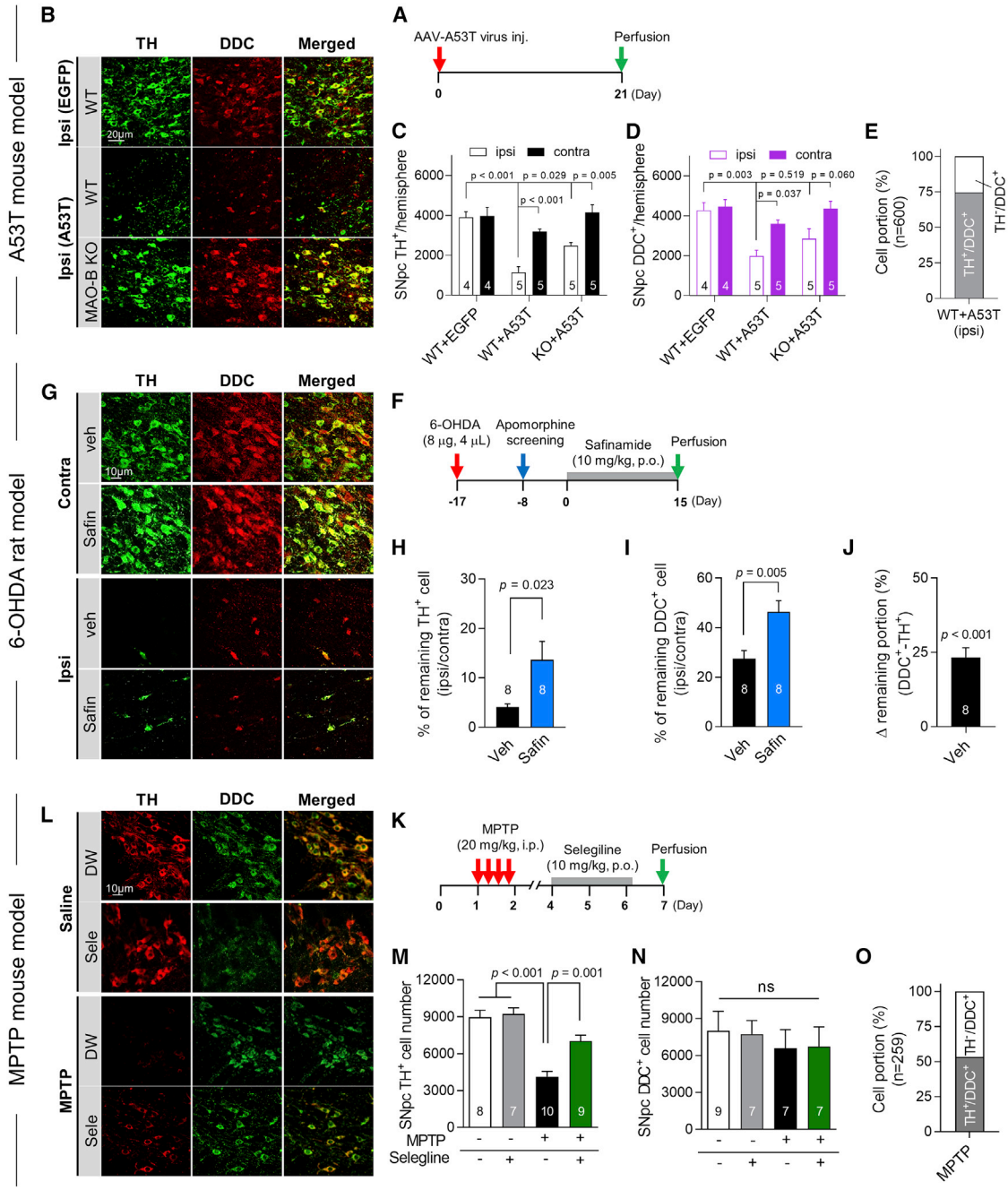

Figure 2. Dormant TH⁻/DDC⁺ Neurons in SNpc of PD Animal Models

(A, F, and K) Experimental timelines.

(B, G, and L) Representative confocal images of TH and DDC double-stained DA neurons in the SNpc of A53T-mutated α-synuclein overexpressed WT or MAO-B KO mice (N = 3, 3, and 5 for respective groups) (B), saline- or safinamide (10 mg/kg/day)-treated 6-OHDA rat models (N = 4 for each group) (G), or saline- or selegiline (10 mg/kg/day)-treated MPTP mouse models (N for each group is indicated on the bar) (L).

(C and D) Number of TH⁺ (C) and DDC⁺ (D) neurons in unilateral SNpc of A53T models.

(E) Portion of TH⁻/DDC⁺ neurons among remaining DDC⁺ neurons in ipsilateral SNpc of A53T model.

(H) Portions of remaining TH⁺ neurons in ipsilateral SNpc compared to contralateral SNpc in 6-OHDA models.

(I) Portions of remaining TH⁺ and DDC⁺ neurons in ipsilateral SNpc compared to contralateral SNpc in 6-OHDA models.

(J) Difference between remaining portions of DDC⁺ neurons and TH⁺ neurons in SNpc of 6-OHDA models.

(M and N) Number of TH⁺ (M) and DDC⁺ (N) neurons in SNpc of MPTP model.

(O) Portion of TH⁻/DDC⁺ neurons among remaining DDC⁺ neurons in SNpc of MPTP model.

Numbers on each bar refer to the numbers of slices (H–J), or animals (C, D, M, and N). For all panels, mean ± SEM; ns, non-significance. Additional statistical details are provided in Table S2. See also Figure S2.

ratio of ipsilateral over contralateral sides, but not on stereological assessment. Therefore, the estimation may not be accurate, and there is a limitation of the interpretation of these results. These findings indicate that MAO-B inhibition can recover dopamine-synthesizing enzymes, TH and DDC. In other words, MAO-B might be the primary cause of the loss of TH and DDC expression, possibly through either MAO-B-mediated neurotoxicity via H_2O_2 production or MAO-B-mediated suppression of TH and DDC expression in DA neurons, or both. In any case, MAO-B could account for suppression of DA neuronal activity and TH loss in the acute PD animal models.

Suppression of SNpc Neuronal Firing by GABA and Disinhibition by MAO-B Inhibition

To test if the DA neuronal firing is indeed suppressed in PD animal models, we performed *in vivo* unit recording from SNpc neurons of anesthetized animals placed on a stereotaxic device, using a recently developed neural probe (Figure 3A) [40]. The *in vivo* DA pacemaker firing in anesthetized mice was previously reported [41]. Because SNpc DA neurons are known to show either a slow, single spiking pattern or burst firing [42], we excluded the neurons with a high-frequency (>10 Hz), single spiking pattern from the analyses. The *in vivo* pacemaker firing rate of putative DA neurons was significantly decreased by about 60% and 76% in MPTP and 6-OHDA models, respectively. These reductions in putative DA neuronal firing rates were significantly and fully rescued by treatment with selegiline in the MPTP model and safinamide in the 6-OHDA model (Figures 3B–3E). In addition, astrocyte-specific gene silencing of MAO-B (Figures S3A–S3D) significantly rescued the firing rates in the MPTP model (Figures 3F and 3G). These findings can be explained by a possible high vulnerability of fast-spiking neurons by the toxins, which can be protected by MAO-B inhibition or suppression of the neuronal firing by MAO-B-mediated tonic inhibition.

To test those possibilities, we performed loose cell-attached patch-clamping on DA neurons in acutely prepared SNpc slices of TH-EGFP mice to measure DA neuronal firing rates without disturbing the intracellular ionic concentration (Figure 3H). Similar to *in vivo* unit recording, we found that the DA pacemaker firing rate was significantly reduced by MPTP treatment, which was significantly restored by MAO-B inhibition via 1-h incubation of SNpc slices with selegiline (100 nM) (Figure 3I). The decreased firing rate was significantly recovered by antagonizing $GABA_A$ receptor via bicuculline (50 μM) treatment in the MPTP model, while bicuculline treatment only showed a non-significant increasing trend of firing rate in the saline-treated mice (Figure 3J). These results indicate that GABA-mediated inhibition of DA neurons causes the suppression of DA pacemaker firing in the PD models.

DA Neurons Are Tonically Inhibited by MAO-B-Dependent GABA in PD Models

The mode of action of GABA can be either phasic or tonic inhibition. To test whether DA neurons are either phasically or tonically inhibited, we performed whole-cell patch-clamp recordings from SNpc DA neurons and measured $GABA_A$ receptor-mediated currents in the presence of ionotropic glutamate receptor antagonists, APV (50 μM) and CNQX (20 μM), as described previously [43]. We found no change in the frequency and amplitude of spontaneous inhibitory postsynaptic currents (sIPSCs) in the A53T mouse model (Figures 4A and 4B). On the other hand, we found an appearance of aberrant tonic GABA current, revealed by treatment with the $GABA_A$ receptor antagonist bicuculline (50 μM), in the ipsilateral SNpc, but not in the contralateral SNpc of the A53T model (Figure 4C). The similar increase in tonic GABA current, but not sIPSCs, was consistently observed in the MPTP and 6-OHDA models (Figures 4D–4J). These results suggest that the increase of tonic GABA current is derived from the astrocytically released GABA. It has been previously shown that astrocytes produce GABA through MAO-B (Figure S7A) [27, 44], which is a mitochondrial enzyme mainly expressed in astrocytes of SNpc [45, 46]. Therefore, we tested if MAO-B inhibition can reverse the aberrant increase of tonic GABA current in the PD models. We found that the increased tonic GABA was reverted to control levels by treating with selegiline or safinamide, whereas these compounds did not alter the tonic GABA current in the contralateral SNpc of the 6-OHDA model and saline-treated control mice (Figures 4F and 4J). In addition, astrocyte-specific gene silencing of MAO-B significantly reduced MPTP-induced excessive tonic GABA current without altering sIPSCs (Figures 4K–4M). Taken together, these results indicate that the DA neurons in SNpc are indeed inhibited by tonically released astrocytic GABA.

The aberrant tonic GABA current was mainly dependent on the $GABA_A$ receptor α5 subunit (Gabra5), as revealed by treatment with an inverse agonist of Gabra5, L655,708 (Figures S3F–S3H). This finding was consistent with a previous report that tonic inhibition in hippocampus is mediated by Gabra5-containing $GABA_A$ receptors [47]. In addition, we found that L655,708 treatment significantly rescued the SNpc neuronal DA firing rate of the MPTP model (Figures S3I–S3K). Our findings indicate that the extrasynaptic $GABA_A$ receptor is indeed responsible for excessive tonic inhibition of DA neuronal firing.

Aberrant Astrocytic GABA to Silence DA Neurons

To directly confirm the astrocytic source of GABA in the SNpc, we performed immunohistochemistry using an antibody against GABA [27]. As previously demonstrated [13, 14], we found that astrocytes in the SNpc became dramatically reactive in the A53T, 6-OHDA, and MPTP models as evidenced by increased GFAP expression, hypertrophy, and marked increase in GABA, while the protein expression of TH was significantly decreased compared to the control groups (Figure 5). The astrocytic changes were also found in rat PD models induced by either A53T [33] or MPP^+ (1-methyl-4-phenylpyridinium) [48] (Figures S4A–S4D). We also found that genetic deletion or pharmacological inhibition of MAO-B showed a significant protection or recovery from astrocytic hypertrophy, aberrant GABA, and decreased TH expression in SNpc neurons of the PD models (Figure 5). Consistently, we found that putrescine and MAO-B, the source and key enzyme of GABA production in astrocytes, respectively (Figure S7A), are overexpressed in the SNpc of various PD animal models (Figures S4E–S4H). These results indicate that MAO-B is the essential enzyme not only for suppression of DA neuronal activity and TH loss, but also for aberrant GABA production. These results imply that MAO-B-dependent aberrant GABA

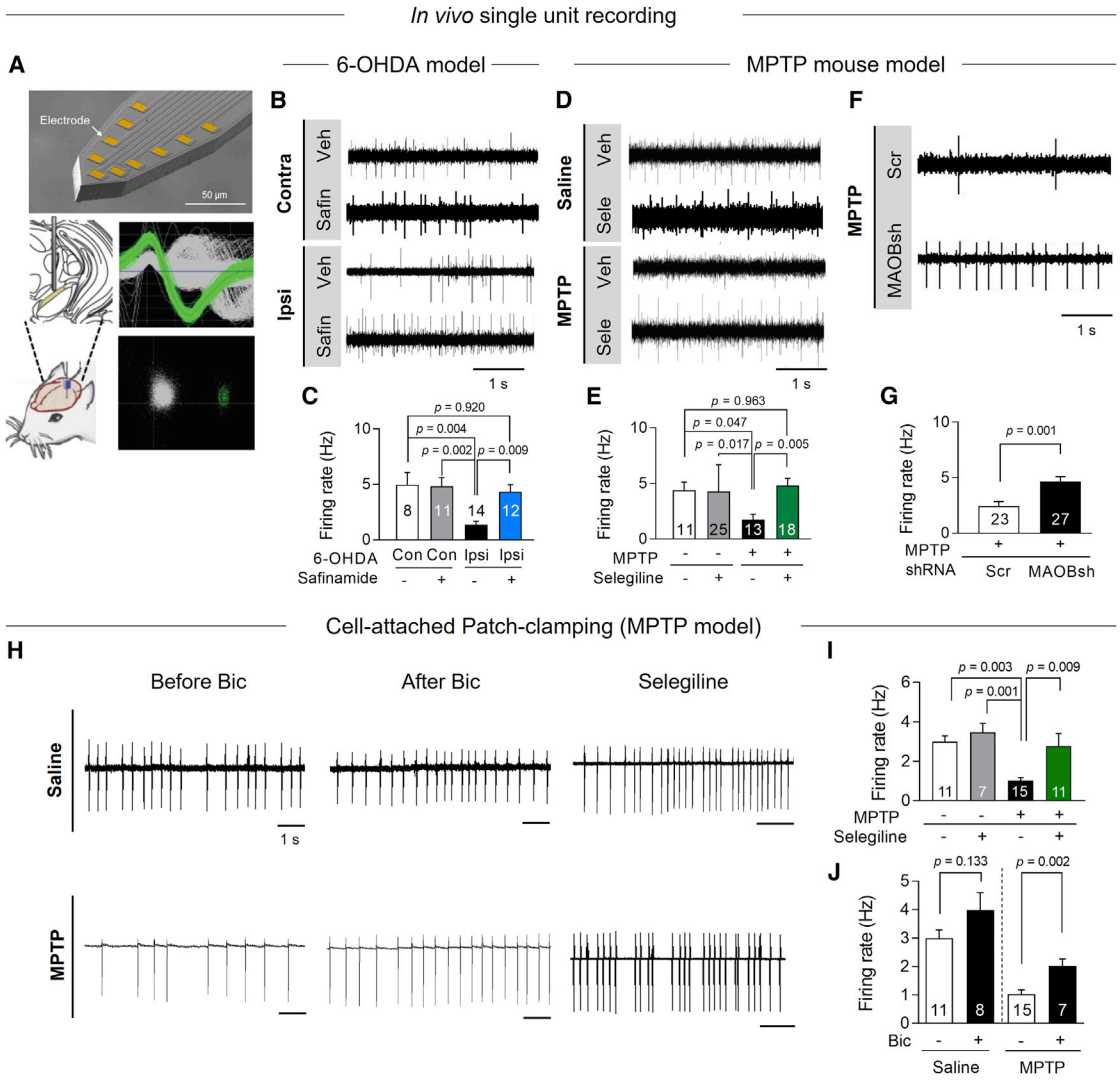

Figure 3. Suppression of DA Neuronal Firing by GABA and Disinhibition by MAO-B Blockade

(A) Top: MEMS neural probe. Bottom left: schematic diagram of *in vivo* single-unit recording. Bottom right: action potential waveforms and single-unit cluster of DA neurons (green) and other neurons (gray).

(B, D, and F) Representative recording traces from the SNpc of live animals (B, N = 4, 5, 5, and 5 for respective groups; D, N = 5 for each group; F, N = 4 for each group).

(C, E, and G) Mean firing rate of DA neurons recorded from SNpc neurons in saline- or safinamide (10 mg/kg/day)-treated 6-OHDA rat models (D), saline- or selegiline (10 mg/kg/day)-treated MPTP mouse models (E), or scrambled-shRNA or MAOB-shRNA-injected MPTP mouse models (G).

(H) Representative traces of spontaneous firing currents recorded from DA neurons of the SNpc in saline, MPTP, and 1 h selegiline pre-treatment for brain slices from MPTP mice (N = 5, 3, 5, and 4 for respective groups).

(I) SNpc neuronal firing rate recorded from MPTP mouse models before and after 1 h incubation with selegiline (100 nM).

(J) SNpc neuronal firing rate before and after bicuculline (Bic, 50 μM) application.

Numbers on each bar refer to the numbers of units (D and E) or cells (H and I). For all panels, mean ± SEM; ns, non-significance. Additional statistical details are provided in Table S2. See also Figure S3.

production is responsible for suppression of DA neuronal activity and TH loss.

As described above, we utilized three different manipulations for inhibiting the action of MAO-B: genetic deletion of MAO-B and pharmacological inhibition of MAO-B by selegiline or safinamide. All of these manipulations significantly blocked astrocytic GABA synthesis, which is associated with parkinsonism. It is consistent with our previous reports that cerebellar astrocytes in MAO-B KO mice cannot normally produce GABA [44, 49] and that long-term treatment of a reversible MAO-B inhibitor significantly blocks astrocytic GABA synthesis [39]. Notably, we treated the animals with selegiline, an irreversible MAO-B inhibitor, for only 3 days, which was demonstrated to markedly block astrocytic GABA synthesis [27], while long-term treatment with selegiline showed no effect [39]. Our findings demonstrate that all of these manipulations for MAO-B inhibition were

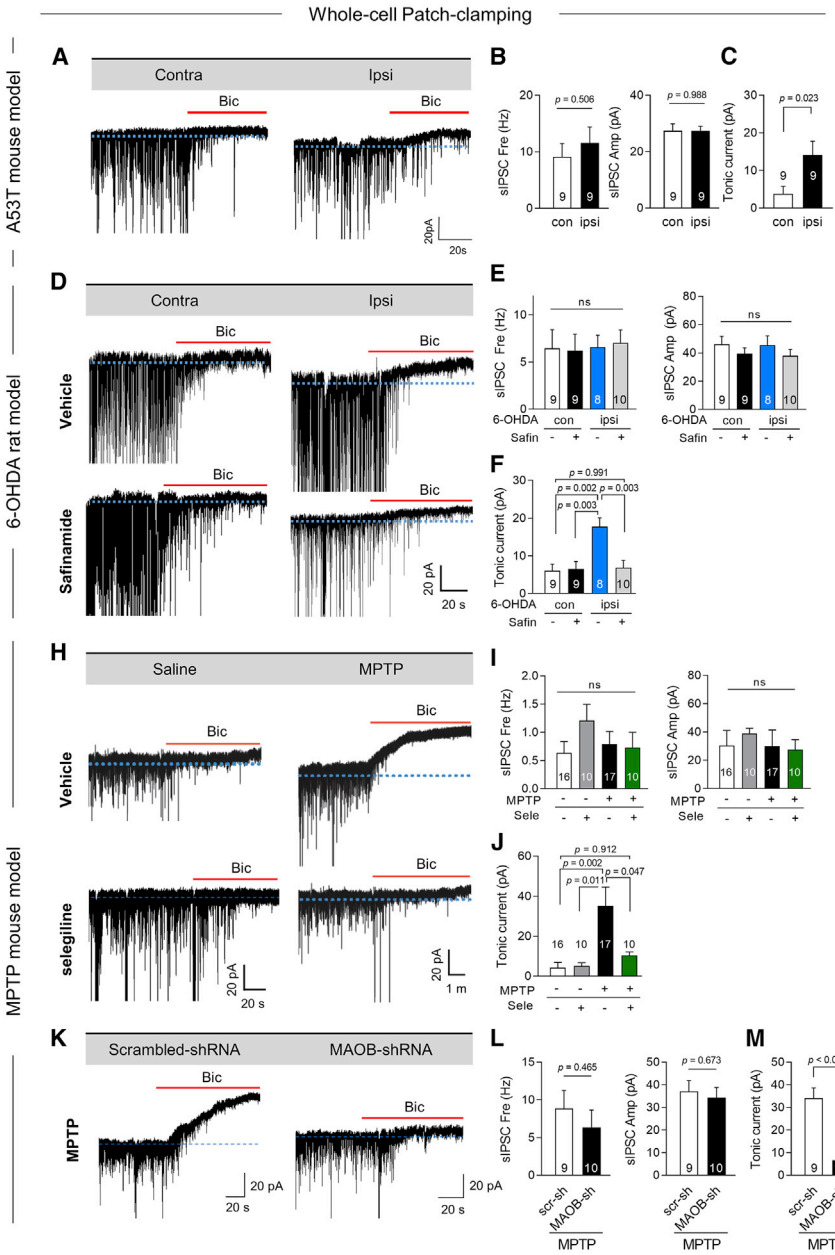

Figure 4. DA Neurons Are Tonically Inhibited by MAO-B-Mediated Aberrant GABA in Acute PD Models

(A, D, H, and K) Representative traces of $GABA_A$ receptor-mediated currents recorded from DA neurons of SNpc of A53T (N = 4 for each group) (A), 6-OHDA (N = 4, 4, 4, and 5 for respective groups) (D), or MPTP (N = 5, 4, 5, and 5 for respective groups) (H and K) PD models. Blue dashed lines indicate baseline shift with bicuculline (Bic, 50 μM) application (red bar).

(B) Frequency and amplitude of sIPSC measured from SNpc DA neurons in the A53T mouse model.

(C) $GABA_A$ receptor-mediated tonic GABA current measured from SNpc DA neurons in the A53T mouse model.

(E, I, and L) Frequency and amplitude of sIPSC measured from SNpc DA neurons in saline- or safinamide (10 mg/kg/day)-treated 6-OHDA rat models (E), saline- or selegiline (10 mg/kg/day)-treated MPTP mouse models (I), or scrambled-shRNA or MAOB-shRNA-injected MPTP mouse models (L).

(F, J, and M) $GABA_A$ receptor-mediated tonic GABA current measured from SNpc DA neurons in 6-OHDA or MPTP models. Numbers on each bar refer to the numbers of cells.

For all panels, mean ± SEM; ns, non-significance. Additional statistical details are provided in Table S2. See also Figure S7.

Aberrant Astrocytic GABA Causes Parkinsonian Motor Symptoms

Next, we tested whether astrocytic GABA is critical for parkinsonian motor symptoms. First, we performed a rotarod test [51] to assess the motor symptoms of the A53T model. We found impaired motor coordination in the A53T model, while MAO-B KO mice showed a resistance to α-synuclein-induced motor symptoms (Figures 6A and 6B). Next, we performed a stepping test to evaluate the motor symptoms in the 6-OHDA rat model [52]. Notably, the motor symptoms in the 6-OHDA model were partially but significantly alleviated by safinamide treatment (Figures 6C and 6D). To assess the motor symptoms of the MPTP model, we utilized a vertical grid test [53], a very sensitive method to detect subtle dopamine-associated motor deficits in the MPTP model (Figures 6E and 6F). We found that selegiline treatment (3 days post-treatment) significantly alleviated MPTP-induced motor symptoms as confirmed by significant reductions in total time, time to turn, and the ratio of missed steps, except for the failure step ratio, which only showed a trend of reduction (Figure 6F). The extent of TH recovery by MAO-B inhibition both in SNpc and striatum was positively correlated with the extent of motor recovery in these animal models (Figures S4M and S4N). Moreover, astrocyte-specific gene silencing of MAO-B in SNpc showed a significant resistance to MPTP-induced motor dysfunction (Figure S3E).

effective in blocking astrocytic GABA synthesis, implying the crucial role of MAO-B in astrocytic GABA in the PD pathology.

We additionally tested if GABA synthesized in the reactive astrocytes needs to be released and accumulated in the extracellular space by performing the sniffer-patch technique (Figure S4I) [50] and high-performance liquid chromatography (HPLC; Figure S4K) [27]. We confirmed that GABA could be released from acutely dissociated SNpc astrocytes of the MPTP model (Figure S4J). We also confirmed the increased extracellular GABA concentration in the SNpc of the MPTP model, which was restored by selective inhibition of MAO-B by selegiline, with no significant alteration in glutamate level (Figure S4L). These results indicate that GABA, synthesized by MAO-B in reactive astrocytes, is released and accumulated in the extracellular space of the SNpc.

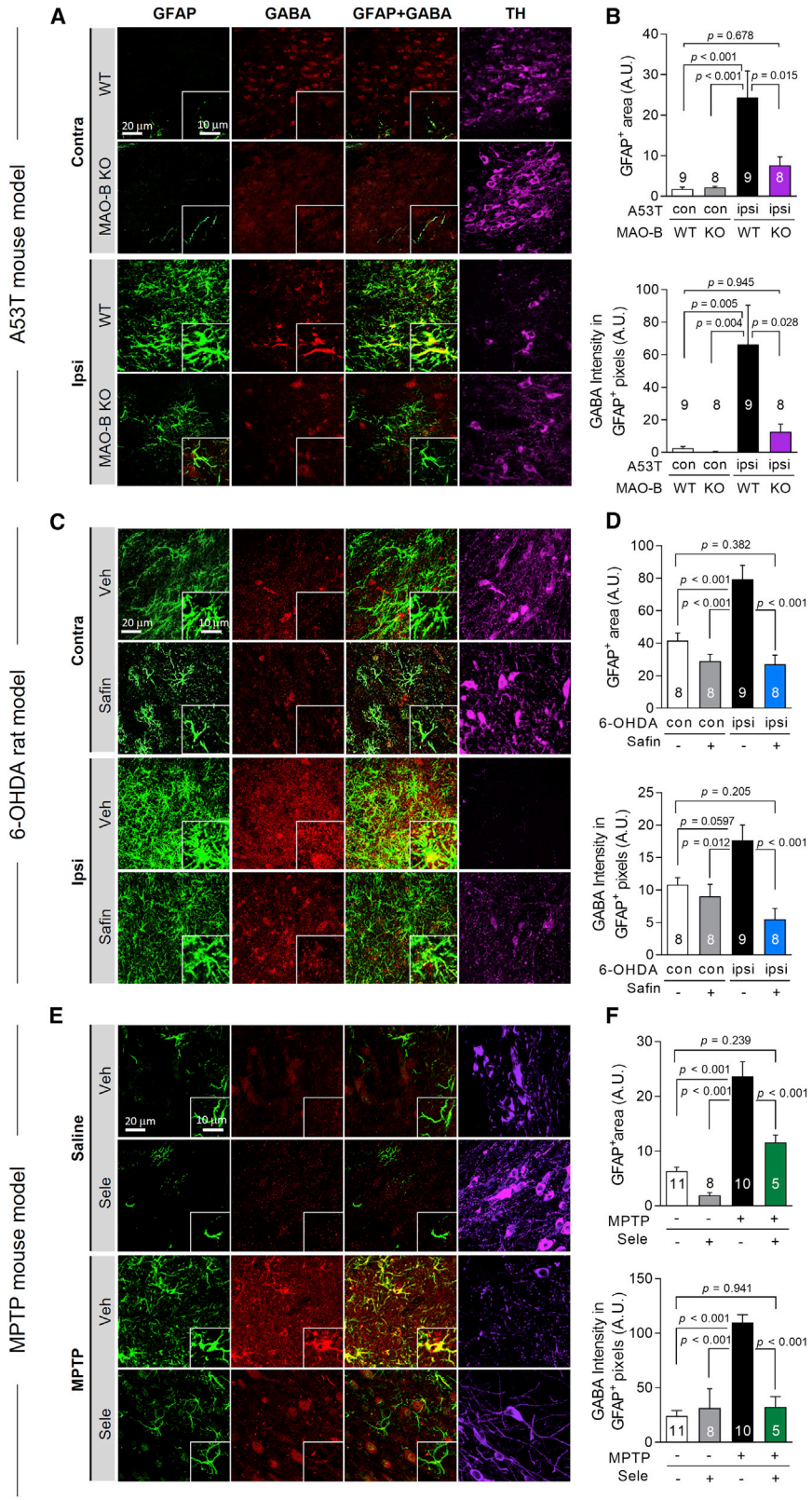

Figure 5. Astrocytic GABA Is Augmented in the SNpc of PD Animal Models

(A, C, and E) Confocal images of GFAP, GABA, and TH in the SNpc of A53T-mutated α-synuclein overexpressed WT or MAO-B KO mice (N = 4 for each group) (A), saline- or safinamide (10 mg/kg/day)-treated 6-OHDA rat models (N = 4 for each group) (C), or saline- or selegiline (10 mg/kg/day)-treated MPTP mouse models (N = 4, 4, 4, and 5 for respective groups) (E).

(B, D, and F) Quantification of GFAP-positive area and GABA intensity in the GFAP-positive pixels. Numbers within each bar refer to the numbers of slices.

For all panels, mean ± SEM, *p < 0.05; **p < 0.01; ***p < 0.001; ns, non-significance. Additional statistical details are provided in Table S2. See also Figures S4 and S7.

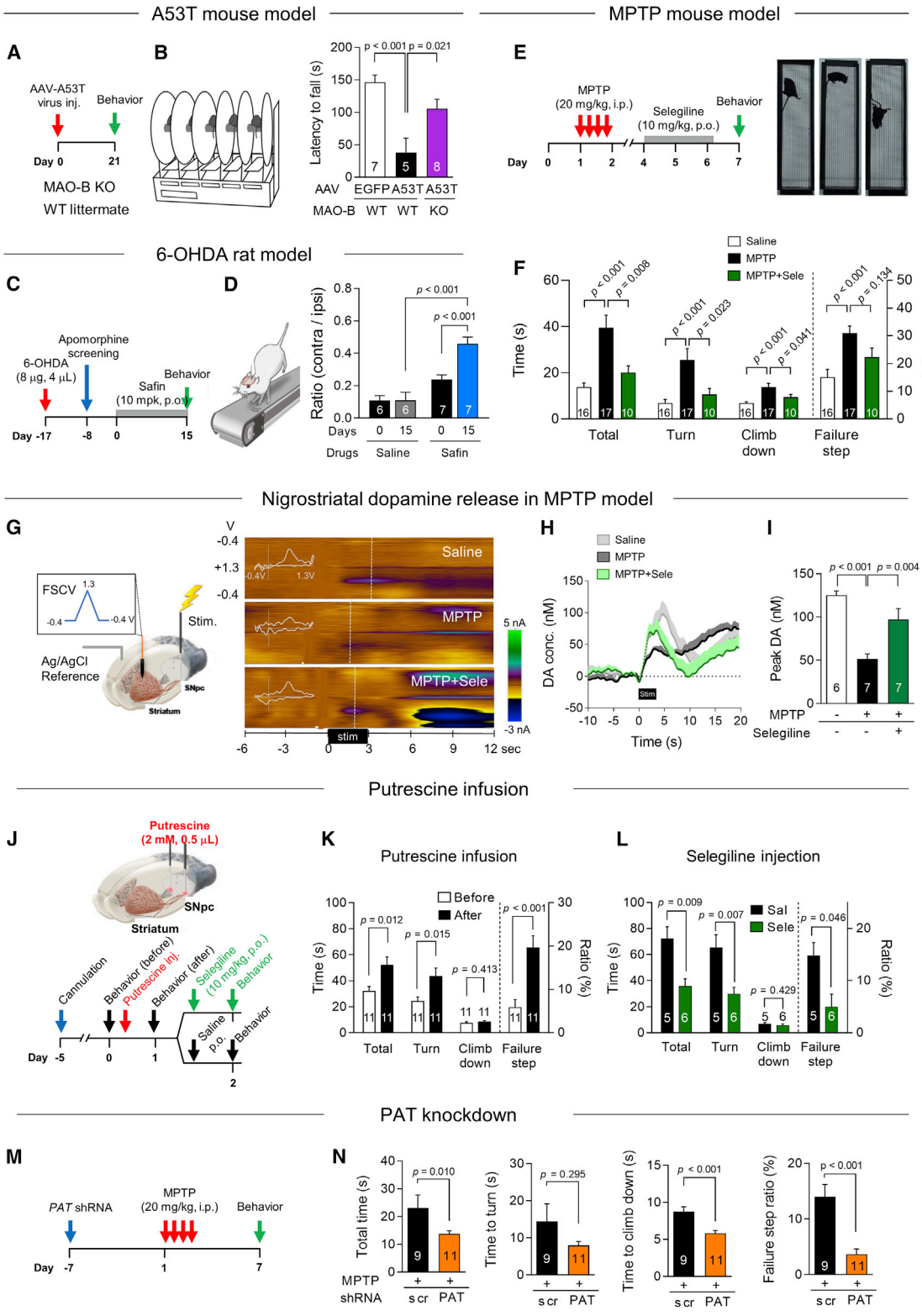

Figure 6. Aberrant Astrocytic GABA Causes Parkinsonian Motor Symptoms

(A) Experimental protocol of behavioral test with A53T mouse model.

(B) Left: schematic diagram of rotarod test. Right: latency-to-fall for rotarod test.

(C) Experimental protocol of behavioral test with 6-OHDA model.

(D) Left: schematic diagram of stepping test. Right: ratio of ipsilateral and contralateral adjusting steps for the stepping test.

(legend continued on next page)

These results indicate that the action of MAO-B, the key enzyme for astrocytic GABA synthesis, is critical for parkinsonian motor symptoms.

To test if this improvement of the motor function by MAO-B inhibition is accompanied by a recovery of nigrostriatal dopamine release, we performed *in vivo* fast-scan cyclic voltammetry (FSCV) with the MPTP mouse model (Figure 6G). We found that dopamine release in dorsal striatum upon electrical SNpc stimulation was significantly reduced in the MPTP model, whereas post-treatment of selegiline significantly recovered the nigrostriatal dopamine release (Figures 6G–6I). These findings were consistent with the results from behavioral assays. Moreover, these results suggest that MAO-B-dependent astrocytic GABA inhibits dopamine synthesis in the SNpc of the MPTP model.

In addition to astrocytic GABA synthesis (Figure S7A), MAO-B has been believed to participate either in conversion of MPTP to MPP+ (Figure S7B) or in degradation of dopamine (Figure S7C). Moreover, MAO-B KO mice were reported to show a resistance to MPTP-induced neurotoxicity [54]. Therefore, the protective effect of genetic deletion or pharmacological inhibition of MAO-B in PD models could be attributed to any one of these possible actions of MAO-B. To bypass the MAO-B's action of MPP+ conversion, we always treated the animals with selegiline 3 days after MPTP treatment. During the 3 days, all of the MPTP should have been converted to MPP+ [55], and any alleviating effect by selegiline should be independent of MAO-B's action of MPP+ conversion. The other possibility that the protective effect in MAO-B KO mice is due to the lack of dopamine degradation is unlikely because MAO-B KO mouse is reported to display an unaltered striatal dopamine level [56]. Taken together, our results indicate that the conventional actions of MAO-B may not be critically involved in the pathophysiology of PD.

If the major action of MAO-B in parkinsonian motor symptoms is through aberrant GABA production, we should be able to mimic the action of MAO-B by manipulating the metabolites and other enzymes of the putrescine degradation pathway leading to GABA production (Figure S7A). First, to induce aberrant GABA production, we bilaterally injected putrescine (2 mM, 0.5 μL), the precursor metabolite of GABA, into the SNpc of healthy mice (Figure 6G). We found that this direct injection of putrescine was sufficient to recapitulate the aberrant astrocytic GABA, reactive gliosis, reduced TH level (Figures S5A–S5C), and parkinsonian motor symptoms, even 1 day after injection (Figure 6H). All these pathological changes were significantly recovered by 1-day selegiline treatment (Figures 6I and S5A–S5C). To mimic the effect of MAO-B inhibition, we gene-silenced putrescine N-acetyltransferase (PAT, also known as diamine acetyltransferase encoded by the *SAT1* gene), the first enzyme of the putrescine degradation pathway (Figure S7A). We developed and injected into the SNpc a lentivirus carrying PAT-specific short hairpin RNA (shRNA), whose knockdown efficiency was confirmed *in vitro* and *in vivo* (Figures 6J and S5D–S5F). Gene silencing of PAT significantly prevented MPTP-induced aberrant astrocytic GABA (Figures S5G–S5I), nigrostriatal TH loss (Figures S5J–S5L), and parkinsonian motor symptoms (Figure 6K). These results establish the causal relationship between the aberrant synthesis of astrocytic GABA via putrescine degradation pathway and parkinsonian motor symptoms, raising several other candidate molecules besides MAO-B for potential therapeutic targets against PD. In addition, blocking the tonic GABA signaling by pharmacological blockade of Gabra5 recovered nigral TH loss and parkinsonian motor symptoms (Figures S3L–S3O). Taken together, blocking astrocytic GABA synthesis leads to reducing tonic inhibition, awakening dormant DA neurons in SNpc, and alleviating parkinsonian motor symptoms.

TH^-/DDC^+ Neurons and Astrocytic GABA in PD Patients

To assess the clinical relevance of astrocytic GABA in PD, we obtained age-matched SNpc brain samples from seven normal individuals and eleven PD patients who were determined as mild or severe PD based on the postmortem examination of midbrain sections by TH immunostaining (Figure 7A; Table S1). We focused on the ventrolateral tier of SNpc (nucleus A9), which is known to be the most vulnerable region of neurodegeneration in PD [57] (Figure 7B). We first assessed the TH and DDC expression separately and found that the number of DDC^+ neurons as well as TH^+ neurons significantly decreased according to the severity of the disease (Figures 7C–7E). Remarkably, in both mild and severe PD patients, the portions of remaining DDC^+ neurons in SNpc compared to normal subjects were greater than those of TH^+ neurons (Figure 7F), raising a possibility that the dormant TH^-/DDC^+ neurons exist. To confirm the existence of the dormant TH^-/DDC^+ neurons, we performed double immunostaining of TH and DDC from each patient group sample (Figure 7G). First, we found that almost all TH^+ neurons were DDC^+ neurons (Figure 7H) and the total number of TH^+/DDC^+ neurons was reduced significantly according to the severity of the disease (Figure 7I). More importantly, we found a significant portion of TH^-/DDC^+ neurons in both mild and severe PD patients (54.7% and 27.0% in mild and severe PD patients, respectively; Figure 7J). These results indicate that the dormant but

(E) Experimental protocol of behavioral test with MPTP mouse model.
(F) Top: schematic diagram of vertical grid. Bottom: total time, time to turn, time to climb down, and failure step ratio for vertical grid test.
(G) Left: schematic diagram of *in vivo* FSCV with MPTP mouse model. Right: representative electrochemical currents in color heat plots as a function of voltage and time.
(H) Changes in calculated dopamine concentration.
(I) Peak dopamine concentration.
(J) Schematic diagram and experimental protocol of *in vivo* putrescine injection into the SNpc and vertical grid test.
(K) Behavioral data from vertical grid test before and after putrescine injection.
(L) Behavioral data from vertical grid test with putrescine-injected mice after saline or selegiline treatment.
(M) Experimental protocol for vertical grid test with *PAT* shRNA injection and MPTP administration.
(N) Behavioral data from vertical grid test.
Numbers within or above each bar refer to the numbers of animals. For all panels, mean ± SEM; ns, non-significance. Additional statistical details are provided in Table S2. See also Figures S5 and S7.

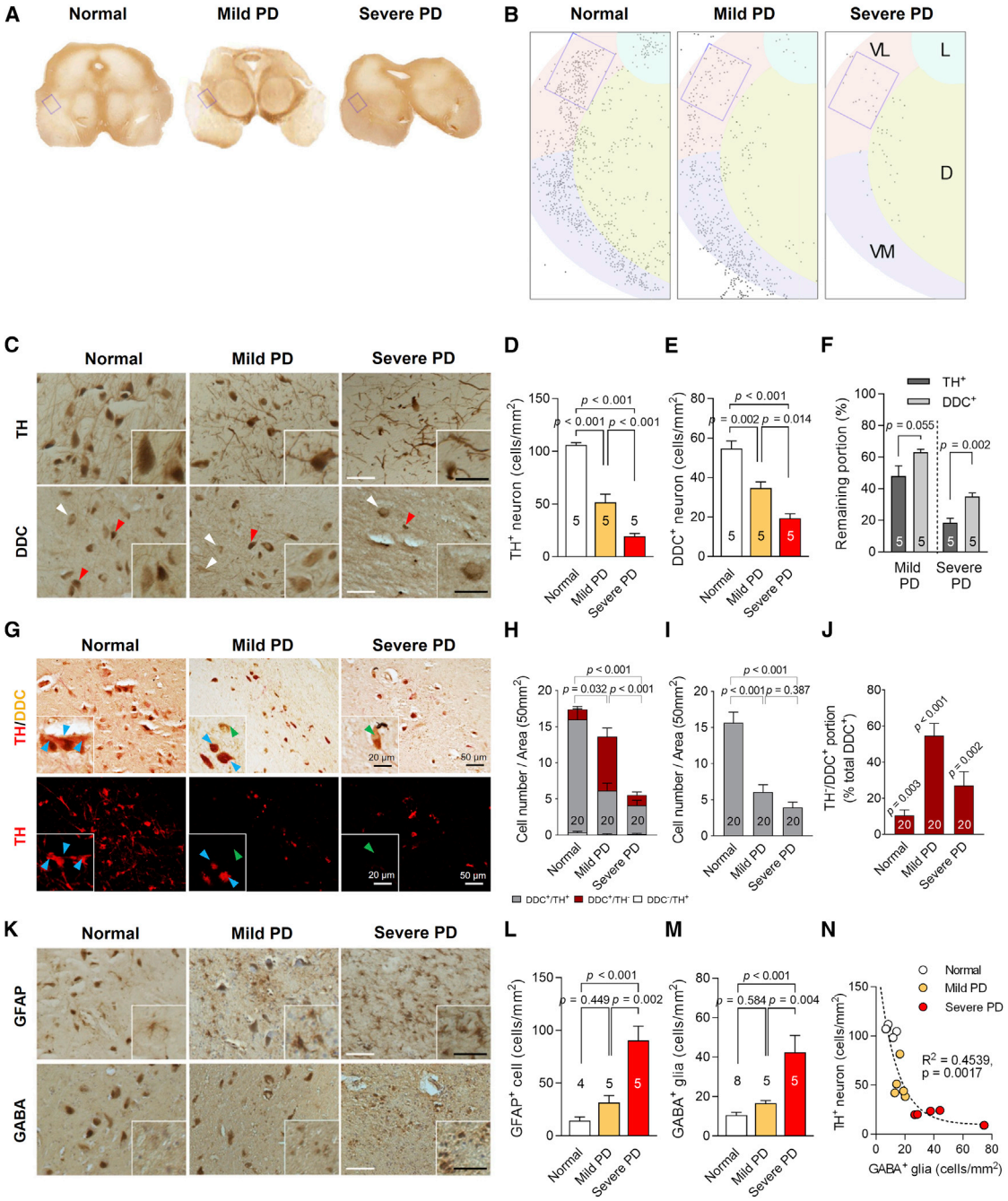

Figure 7. TH⁻/DDC⁺ Neurons and Astrocytic GABA in PD Patients

(A) Representative SNpc tissues of normal and PD (mild and severe) human subjects.

(B) Mapping neuromelanin⁺ DA neurons in the SNpc (nucleus A9). Regions of interest are indicated by rectangles. VL, ventrolateral tier; VM, ventromedial tier; D, dorsal tier; L, pars lateralis.

(C) Representative immunohistochemistry images of TH and DDC in the VL of SNpc. Note that DDC⁺/neuromelanin⁻ neurons (white arrowheads) can be distinguished from both positive neurons (red arrowheads) by color.

(D and E) Quantification of the decrease of TH⁺ and DDC⁺ neurons.

(F) Remaining portion of DDC⁺ and TH⁺ neurons in mild and severe PD patients, compared to normal subjects.

(G) Representative images of TH and DDC double-immunostaining in the VL of SNpc.

(H and I) Quantification of TH⁺ and/or DDC⁺ cell numbers.

(J) The portion of TH⁻/DDC⁺ neurons out of total DDC⁺ neurons.

(K) Representative immunohistochemistry images of GFAP and GABA in the VL of SNpc. Note that neuromelanin⁺ DA neurons (dark brown) can be distinguished from GFAP⁺/GABA⁺ glial cells (light brown) by color and cell shape.

(legend continued on next page)

recoverable TH^-/DDC^+ neurons are still alive in the SNpc of PD patients.

We next examined the level of GFAP and GABA in this region using immunohistochemistry (Figures 7K and S6A). Consistent with the results from animal PD models, we found a significant increase in the number of GFAP-positive ($GFAP^+$) and GABA-positive ($GABA^+$) glia in the ventrolateral SNpc, and this increase positively correlated with the severity of the disease (Figures 7L and 7M). The mRNA levels of GFAP and MAO-B in the SNpc of severe PD subjects were also significantly higher than those of control subjects (Figure S6B). These results indicate that astrocytes become reactive and astrocytic GABA synthesis is increased in SNpc of PD patients. The number of $GABA^+$ glia was inversely correlated with the number of TH^+ DA neurons, suggesting that astrocytic GABA is critically involved in the pathology of PD (Figure 7N). Similarly, using the neuromelanin, a well-known marker for DA neurons, we confirmed both a greater remaining portion of DDC^+ neurons compared to that of neuromelanin-positive ($neuromelanin^+$) neurons and a strong inverse correlation between numbers of $GABA^+$ glia and $neuromelanin^+$ neurons (Figures S6C–S6E). Taken together, these dormant TH^-/DDC^+ neurons might be strongly suppressed by GABA from reactive astrocytes, and awakening of these remaining neurons could be an effective therapeutic strategy to relieve parkinsonian motor symptoms in PD.

DISCUSSION

In the current study, we provide unprecedented evidence for a non-cell-autonomous mechanism of astroglial change that is the critical factor of DA neuronal dysfunction, which can result in PD motor symptoms. We demonstrate that astrocytes in the SNpc of PD model animals and PD patients become reactive and produce GABA via the putrescine degradation pathway. The released GABA strongly inhibits firing of SNpc neurons including DA neurons. Thus, GABA from reactive astrocytes has two important effects: it diminishes dopamine release in the nigrostriatal pathway by inhibiting firing and dopamine production by downregulating the TH expression [6–8], both of which can lead to parkinsonian motor symptoms (Figure S7D). Our study provides the first insight into non-cell-autonomous causes of PD motor symptoms: reactive astrocytes are actively involved in glia-neuron interactions by releasing the inhibitory gliotransmitter, GABA, which works in concert with other pathological factors to alter the activity of neural networks in the PD brain.

One of the most striking observations from this study is the existence of a significant portion of TH^-/DDC^+ dormant DA neurons in the diseased SNpc. These TH^-/DDC^+ neurons could be transitional neurons that are bound to die as they appear to be undergoing atrophy (Figure S2K). Or they could be the surviving neurons that respond robustly to L-DOPA treatments, actively converting L-DOPA to dopamine via the remaining DDC enzyme. Regardless of whether they are dying or surviving, we propose that these dormant DA neurons could be the prime therapeutic target for the neuromodulation to restore the TH expression and motor function in PD.

We have demonstrated that pharmacological inhibition and genetic deletion of MAO-B have significant therapeutic effects in animal models of PD, even though there is a limitation of this study: we did not test whether selegiline treatment causes any changes in behavior and dopamine level in the WT animals. Overall, our study proposes MAO-B inhibition as a potential disease-modifying therapeutic strategy for patients with early-stage PD through disinhibition of the dormant dopaminergic neurons. However, the results from several clinical trials have cast doubt on the therapeutic efficacy of traditional irreversible MAO-B inhibitors such as selegiline and rasagiline on PD [58–60]. These discrepancies can be fully explained by our very recent findings that long-term use of the irreversible MAO-B inhibitors undesirably turns on the compensatory mechanisms for GABA production through an increase in the expression and activity of an alternative GABA-synthesizing enzyme, diamine oxidase [39]. Fortunately, we have recently developed a new class of a potent, selective, and reversible MAO-B inhibitor, KDS2010, that effectively inhibits astrocytic GABA synthesis to fully rescue neuronal firing with minimal undesirable effects in Alzheimer's disease (AD) animal models [39]. We anticipate that this new compound will also be effective for alleviating parkinsonian motor symptoms of PD animal models as well as patients.

MAO-B is also well known to reduce oxygen to hydrogen peroxide when catalyzing oxidative deamination of monoamines [61], resulting in increased mitochondrial oxidative stress, which triggers the neurodegeneration. Indeed, it has been previously reported that overexpression of astrocytic MAO-B induced astrogliosis and elevated hydrogen peroxide level that oxidizes dopamine to dopaminochrome, which in turn elevates mitochondrial superoxide levels in DA neurons [62]. In accordance with this idea, we here demonstrated that scavenging reactive oxygen species significantly impedes MPTP-induced neurodegeneration (Figures S2H–S2J). In summary, the elevated MAO-B activity in reactive astrocytes in the SNpc of PD patients can induce both GABA-mediated neuronal dysfunction through inhibition of DA neuronal firing and reactive oxygen species-mediated neurodegeneration. Therefore, it is possible that long-acting, selective, and reversible MAO-B inhibitors can not only relieve parkinsonian motor symptoms by blocking astrocytic GABA synthesis, but also prevent neurodegeneration by reducing oxidative stress.

The appearance of reactive astrocytes is a prominent feature of not only PD but also many other brain diseases including AD, Huntington's disease, amyotrophic lateral sclerosis, multiple sclerosis, traumatic brain injury, and stroke [63]. However, the role of these reactive astrocytes has been restricted to neuroinflammation or metabolic support. Our study suggests that the interaction between astrocytes and neurons via the strong inhibitory gliotransmitter GABA from reactive astrocytes is a critical factor in PD progression. Furthermore, we propose that targeting

(L and M) Quantification of the increase of $GFAP^+$ and $GABA^+$ glia.

(N) Correlation between number of $GABA^+$ glia and that of remaining TH^+ DA neurons.

Numbers on each bar refer to the numbers of subjects (D–F, J, and K) or ROIs (H–J). For all panels, mean ± SEM; ns, non-significance. Additional statistical details are provided in Table S2. See also Figure S6 and Table S1.

and reducing astrocytic GABA might be beneficial for treating the disease. We expect that future research will unravel previously unknown functions of reactive astrocytes in the etiology of various neuroinflammatory brain diseases.

STAR★METHODS

Detailed methods are provided in the online version of this paper and include the following:

- KEY RESOURCES TABLE
- LEAD CONTACT AND MATERIALS AVAILABILITY
- EXPERIMENTAL MODEL AND SUBJECT DETAILS
  - Animals
  - MPTP mouse model
  - 6-OHDA rat model
  - α-synuclein mouse or rat model
  - MPP+ rat model
  - Human brain samples
- METHOD DETAILS
  - Optogenetics
  - Behavioral tests
  - DAB staining for TH and DDC
  - Slice immunostaining for confocal microscopy
  - PI staining *in vivo*
  - Virus and putrescine injection
  - *In vivo* fast-scan cyclic voltammetry
  - *In vivo* microdialysis
  - L-glutamate and γ-butyric acid measurement
  - Quantitative real-time PCR
  - Measurements of MAO-B enzyme activity
  - Sniffer patch with acutely dissociated astrocytes
  - Tonic GABA recording
  - Cell-attached patch-clamp
  - *In vivo* unit recording
- QUANTIFICATION AND STATISTICAL ANALYSIS
  - Image quantification
  - Stereology
  - Statistical analyses
- DATA AND CODE AVAILABILITY

SUPPLEMENTAL INFORMATION

Supplemental Information can be found online at https://doi.org/10.1016/j.cub.2019.11.079.

ACKNOWLEDGMENTS

The AAV-A53T viral vector was kindly provided by Dr. Jun-ichi Miyazaki at Kumamoto University. This work was supported by the Creative Research Initiative Program (2015R1A3A2066619) of the National Research Foundation (NRF) of Korea funded by the Ministry of Science and ICT of Korea and Institute for Basic Science (IBS), Center for Cognition and Sociality (IBS-R001-D2) to C.J.L.; Asan Life Science Institute grants (18-241 and 19-241) funded by the Asan Medical Center to S.R.J.; Brain Science Program (2018M3C7A1056894) funded by NRF of Korea to H.R.; KIST institutional program (Project No. 2E29221) and Brain Science Program (2018M3C7A1056897) funded by the NRF of Korea to M.H.N.; MRC program (2017R1A5A2015385) funded by the Ministry of Science and ICT of Korea to J.Y.H.; and KBRI basic research program (20-BR-02-05) through Korea Brain Research Institute funded by the Ministry of Science and ICT of Korea to J.K.

AUTHOR CONTRIBUTIONS

Conceptualization, J.Y.H., M.-H.N., H.R., S.R.J., and C.J.L.; Methodology, S.H.H., S.J., J.Y.J., K.I.K., D.-P.J., and S.H.P.; Investigation, J.Y.H., M.-H.N., H.H.Y., J.K., Y.J.H., W.W., J.A.L., D.H.W., M.J.L., S.K., S.J., H.Y.K., J.-E.S., J.H.Y., and H.-J.P.; Resources, K.D.P., B.K. Jin, E.M.H., J.L., N.W.K., H.R., H.J.L., H.S., S.-J.O., S.E.L., and I.-J.C.; Writing – Original Draft, M.H.N. and C.J.L.; Writing – Review & Editing, M.-H.N., J.Y.H., J.K., and C.J.L.; Visualization, M.-H.N. and J.K.; Supervision, O.H., B.K. Jin, S.H.P., G.R.K., I.S., H.R., S.R.J., and C.J.L.; Funding Acquisition, J.Y.H., M.-H.N., J.K., H.R., S.R.J., and C.J.L.

DECLARATION OF INTERESTS

The authors declare no competing financial interests.

Received: September 3, 2019
Revised: October 19, 2019
Accepted: November 26, 2019
Published: January 9, 2020

REFERENCES

1. Dickson, D.W. (2012). Parkinson's disease and parkinsonism: neuropathology. Cold Spring Harb. Perspect. Med. *2*, https://doi.org/10.1101/cshperspect.a009258.
2. Armon, C., Shin, C., Miller, P., Carwile, S., Brown, E., Edinger, J.D., and Paul, R.G. (1996). Reversible parkinsonism and cognitive impairment with chronic valproate use. Neurology *47*, 626–635.
3. Santos, A.F., Rodrigues, M., Abreu, P., and Ferreira, C. (2015). Reversible parkinsonism and cognitive deficits due to vitamin B_{12} deficiency. Neurol. Sci. *36*, 1031–1032.
4. Okada, K., Nomura, M., Furusyo, N., Otaguro, S., Nabeshima, S., and Hayashi, J. (2005). Amelioration of extrapontine myelinolysis and reversible parkinsonism in a patient with asymptomatic hypopituitarism. Intern. Med. *44*, 739–742.
5. Guan, J., Lu, Z., and Zhou, Q. (2012). Reversible parkinsonism due to involvement of substantia nigra in Epstein-Barr virus encephalitis. Mov. Disord. *27*, 156–157.
6. Joh, T.H., Park, D.H., and Reis, D.J. (1978). Direct phosphorylation of brain tyrosine hydroxylase by cyclic AMP-dependent protein kinase: mechanism of enzyme activation. Proc. Natl. Acad. Sci. USA *75*, 4744–4748.
7. Kilbourne, E.J., Nankova, B.B., Lewis, E.J., McMahon, A., Osaka, H., Sabban, D.B., and Sabban, E.L. (1992). Regulated expression of the tyrosine hydroxylase gene by membrane depolarization. Identification of the responsive element and possible second messengers. J. Biol. Chem. *267*, 7563–7569.
8. Aumann, T.D., Egan, K., Lim, J., Boon, W.C., Bye, C.R., Chua, H.K., Baban, N., Parish, C.L., Bobrovskaya, L., Dickson, P., and Horne, M.K. (2011). Neuronal activity regulates expression of tyrosine hydroxylase in adult mouse substantia nigra pars compacta neurons. J. Neurochem. *116*, 646–658.
9. Qi, C., Varga, S., Oh, S.J., Lee, C.J., and Lee, D. (2017). Optogenetic rescue of locomotor dysfunction and dopaminergic degeneration caused by alpha-synuclein and EKO genes. Exp. Neurobiol. *26*, 97–103.
10. Saari, L., Kivinen, K., Gardberg, M., Joutsa, J., Noponen, T., and Kaasinen, V. (2017). Dopamine transporter imaging does not predict the number of nigral neurons in Parkinson disease. Neurology *88*, 1461–1467.
11. Chen, M.K., Kuwabara, H., Zhou, Y., Adams, R.J., Brasić, J.R., McGlothan, J.L., Verina, T., Burton, N.C., Alexander, M., Kumar, A., et al. (2008). VMAT2 and dopamine neuron loss in a primate model of Parkinson's disease. J. Neurochem. *105*, 78–90.
12. Bellucci, A., Antonini, A., Pizzi, M., and Spano, P. (2017). The end is the beginning: Parkinson's disease in the light of brain imaging. Front. Aging Neurosci. *9*, 330.

13. McGeer, P.L., and McGeer, E.G. (2008). Glial reactions in Parkinson's disease. Mov. Disord. *23*, 474–483.
14. Liberatore, G.T., Jackson-Lewis, V., Vukosavic, S., Mandir, A.S., Vila, M., McAuliffe, W.G., Dawson, V.L., Dawson, T.M., and Przedborski, S. (1999). Inducible nitric oxide synthase stimulates dopaminergic neurodegeneration in the MPTP model of Parkinson disease. Nat. Med. *5*, 1403–1409.
15. L'Episcopo, F., Tirolo, C., Testa, N., Caniglia, S., Morale, M.C., Cossetti, C., D'Adamo, P., Zardini, E., Andreoni, L., Ihekwaba, A.E., et al. (2011). Reactive astrocytes and Wnt/β-catenin signaling link nigrostriatal injury to repair in 1-methyl-4-phenyl-1,2,3,6-tetrahydropyridine model of Parkinson's disease. Neurobiol. Dis. *41*, 508–527.
16. Hirsch, E.C., Breidert, T., Rousselet, E., Hunot, S., Hartmann, A., and Michel, P.P. (2003). The role of glial reaction and inflammation in Parkinson's disease. Ann. N Y Acad. Sci. *991*, 214–228.
17. Joe, E.H., Choi, D.J., An, J., Eun, J.H., Jou, I., and Park, S. (2018). Astrocytes, microglia, and Parkinson's disease. Exp. Neurobiol. *27*, 77–87.
18. Hennessy, E., Griffin, E.W., and Cunningham, C. (2015). Astrocytes are primed by chronic neurodegeneration to produce exaggerated chemokine and cell infiltration responses to acute stimulation with the cytokines IL-1β and TNF-α. J. Neurosci. *35*, 8411–8422.
19. Tao, J., Wu, H., Lin, Q., Wei, W., Lu, X.H., Cantle, J.P., Ao, Y., Olsen, R.W., Yang, X.W., Mody, I., et al. (2011). Deletion of astroglial Dicer causes non-cell-autonomous neuronal dysfunction and degeneration. J. Neurosci. *31*, 8306–8319.
20. Di Giorgio, F.P., Carrasco, M.A., Siao, M.C., Maniatis, T., and Eggan, K. (2007). Non-cell autonomous effect of glia on motor neurons in an embryonic stem cell-based ALS model. Nat. Neurosci. *10*, 608–614.
21. Bi, F., Huang, C., Tong, J., Qiu, G., Huang, B., Wu, Q., Li, F., Xu, Z., Bowser, R., Xia, X.G., and Zhou, H. (2013). Reactive astrocytes secrete lcn2 to promote neuron death. Proc. Natl. Acad. Sci. USA *110*, 4069–4074.
22. Lee, H.J., Suk, J.E., Patrick, C., Bae, E.J., Cho, J.H., Rho, S., Hwang, D., Masliah, E., and Lee, S.J. (2010). Direct transfer of alpha-synuclein from neuron to astroglia causes inflammatory responses in synucleinopathies. J. Biol. Chem. *285*, 9262–9272.
23. Fellner, L., Irschick, R., Schanda, K., Reindl, M., Klimaschewski, L., Poewe, W., Wenning, G.K., and Stefanova, N. (2013). Toll-like receptor 4 is required for α-synuclein dependent activation of microglia and astroglia. Glia *61*, 349–360.
24. Sun, L., Shen, R., Agnihotri, S.K., Chen, Y., Huang, Z., and Büeler, H. (2018). Lack of PINK1 alters glia innate immune responses and enhances inflammation-induced, nitric oxide-mediated neuron death. Sci. Rep. *8*, 383.
25. Waak, J., Weber, S.S., Waldenmaier, A., Görner, K., Alunni-Fabbroni, M., Schell, H., Vogt-Weisenhorn, D., Pham, T.T., Reumers, V., Baekelandt, V., et al. (2009). Regulation of astrocyte inflammatory responses by the Parkinson's disease-associated gene DJ-1. FASEB J. *23*, 2478–2489.
26. Filichia, E., Hoffer, B., Qi, X., and Luo, Y. (2016). Inhibition of Drp1 mitochondrial translocation provides neural protection in dopaminergic system in a Parkinson's disease model induced by MPTP. Sci. Rep. *6*, 32656.
27. Jo, S., Yarishkin, O., Hwang, Y.J., Chun, Y.E., Park, M., Woo, D.H., Bae, J.Y., Kim, T., Lee, J., Chun, H., et al. (2014). GABA from reactive astrocytes impairs memory in mouse models of Alzheimer's disease. Nat. Med. *20*, 886–896.
28. Wu, Z., Guo, Z., Gearing, M., and Chen, G. (2014). Tonic inhibition in dentate gyrus impairs long-term potentiation and memory in an Alzheimer's [corrected] disease model. Nat. Commun. *5*, 4159.
29. Oh, S.J., and Lee, C.J. (2017). Distribution and function of the bestrophin-1 (Best1) channel in the brain. Exp. Neurobiol. *26*, 113–121.
30. Chun, H., An, H., Lim, J., Woo, J., Lee, J., Ryu, H., and Lee, C.J. (2018). Astrocytic proBDNF and tonic GABA distinguish active versus reactive astrocytes in hippocampus. Exp. Neurobiol. *27*, 155–170.
31. Cereda, E., Cilia, R., Canesi, M., Tesei, S., Mariani, C.B., Zecchinelli, A.L., and Pezzoli, G. (2017). Efficacy of rasagiline and selegiline in Parkinson's disease: a head-to-head 3-year retrospective case-control study. J. Neurol. *264*, 1254–1263.
32. Zhang, F., Wang, L.P., Brauner, M., Liewald, J.F., Kay, K., Watzke, N., Wood, P.G., Bamberg, E., Nagel, G., Gottschalk, A., and Deisseroth, K. (2007). Multimodal fast optical interrogation of neural circuitry. Nature *446*, 633–639.
33. Sato, H., Arawaka, S., Hara, S., Fukushima, S., Koga, K., Koyama, S., and Kato, T. (2011). Authentically phosphorylated α-synuclein at Ser129 accelerates neurodegeneration in a rat model of familial Parkinson's disease. J. Neurosci. *31*, 16884–16894.
34. Niwa, H., Yamamura, K., and Miyazaki, J. (1991). Efficient selection for high-expression transfectants with a novel eukaryotic vector. Gene *108*, 193–199.
35. Schwarting, R.K., and Huston, J.P. (1996). The unilateral 6-hydroxydopamine lesion model in behavioral brain research. Analysis of functional deficits, recovery and treatments. Prog. Neurobiol. *50*, 275–331.
36. Boyden, E.S., Zhang, F., Bamberg, E., Nagel, G., and Deisseroth, K. (2005). Millisecond-timescale, genetically targeted optical control of neural activity. Nat. Neurosci. *8*, 1263–1268.
37. Jackson-Lewis, V., and Przedborski, S. (2007). Protocol for the MPTP mouse model of Parkinson's disease. Nat. Protoc. *2*, 141–151.
38. Grimsby, J., Toth, M., Chen, K., Kumazawa, T., Klaidman, L., Adams, J.D., Karoum, F., Gal, J., and Shih, J.C. (1997). Increased stress response and beta-phenylethylamine in MAOB-deficient mice. Nat. Genet. *17*, 206–210.
39. Park, J.-H., Ju, Y.H., Choi, J.W., Song, H.J., Jang, B.K., Woo, J., Chun, H., Kim, H.J., Shin, S.J., Yarishkin, O., et al. (2019). Newly developed reversible MAO-B inhibitor circumvents the shortcomings of irreversible inhibitors in Alzheimer's disease. Sci. Adv. *5*, v0316.
40. Lee, H.J., Son, Y., Kim, J., Lee, C.J., Yoon, E.S., and Cho, I.J. (2015). A multichannel neural probe with embedded microfluidic channels for simultaneous in vivo neural recording and drug delivery. Lab Chip *15*, 1590–1597.
41. Schiemann, J., Schlaudraff, F., Klose, V., Bingmer, M., Seino, S., Magill, P.J., Zaghloul, K.A., Schneider, G., Liss, B., and Roeper, J. (2012). K-ATP channels in dopamine substantia nigra neurons control bursting and novelty-induced exploration. Nat. Neurosci. *15*, 1272–1280.
42. Grace, A.A., and Bunney, B.S. (1984). The control of firing pattern in nigral dopamine neurons: single spike firing. J. Neurosci. *4*, 2866–2876.
43. Lee, S., Yoon, B.E., Berglund, K., Oh, S.J., Park, H., Shin, H.S., Augustine, G.J., and Lee, C.J. (2010). Channel-mediated tonic GABA release from glia. Science *330*, 790–796.
44. Yoon, B.E., Woo, J., Chun, Y.E., Chun, H., Jo, S., Bae, J.Y., An, H., Min, J.O., Oh, S.J., Han, K.S., et al. (2014). Glial GABA, synthesized by monoamine oxidase B, mediates tonic inhibition. J. Physiol. *592*, 4951–4968.
45. Levitt, P., Pintar, J.E., and Breakefield, X.O. (1982). Immunocytochemical demonstration of monoamine oxidase B in brain astrocytes and serotonergic neurons. Proc. Natl. Acad. Sci. USA *79*, 6385–6389.
46. Riederer, P., Konradi, C., Schay, V., Kienzl, E., Birkmayer, G., Danielczyk, W., Sofic, E., and Youdim, M.B. (1987). Localization of MAO-A and MAO-B in human brain: a step in understanding the therapeutic action of L-deprenyl. Adv. Neurol. *45*, 111–118.
47. Caraiscos, V.B., Elliott, E.M., You-Ten, K.E., Cheng, V.Y., Belelli, D., Newell, J.G., Jackson, M.F., Lambert, J.J., Rosahl, T.W., Wafford, K.A., et al. (2004). Tonic inhibition in mouse hippocampal CA1 pyramidal neurons is mediated by alpha5 subunit-containing gamma-aminobutyric acid type A receptors. Proc. Natl. Acad. Sci. USA *101*, 3662–3667.
48. Park, E.S., Kim, S.R., and Jin, B.K. (2012). Transient receptor potential vanilloid subtype 1 contributes to mesencephalic dopaminergic neuronal survival by inhibiting microglia-originated oxidative stress. Brain Res. Bull. *89*, 92–96.
49. Woo, J., Min, J.O., Kang, D.S., Kim, Y.S., Jung, G.H., Park, H.J., Kim, S., An, H., Kwon, J., Kim, J., et al. (2018). Control of motor coordination by astrocytic tonic GABA release through modulation of excitation/inhibition balance in cerebellum. Proc. Natl. Acad. Sci. USA *115*, 5004–5009.

50. Woo, D.H., Han, K.S., Shim, J.W., Yoon, B.E., Kim, E., Bae, J.Y., Oh, S.J., Hwang, E.M., Marmorstein, A.D., Bae, Y.C., et al. (2012). TREK-1 and Best1 channels mediate fast and slow glutamate release in astrocytes upon GPCR activation. Cell *151*, 25–40.

51. Iancu, R., Mohapel, P., Brundin, P., and Paul, G. (2005). Behavioral characterization of a unilateral 6-OHDA-lesion model of Parkinson's disease in mice. Behav. Brain Res. *162*, 1–10.

52. Yoon, H.H., Park, J.H., Kim, Y.H., Min, J., Hwang, E., Lee, C.J., Suh, J.K., Hwang, O., and Jeon, S.R. (2014). Optogenetic inactivation of the subthalamic nucleus improves forelimb akinesia in a rat model of Parkinson disease. Neurosurgery *74*, 533–540, discussion 540–541.

53. Kim, S.T., Son, H.J., Choi, J.H., Ji, I.J., and Hwang, O. (2010). Vertical grid test and modified horizontal grid test are sensitive methods for evaluating motor dysfunctions in the MPTP mouse model of Parkinson's disease. Brain Res. *1306*, 176–183.

54. Shih, J.C., Chen, K., and Ridd, M.J. (1999). Monoamine oxidase: from genes to behavior. Annu. Rev. Neurosci. *22*, 197–217.

55. Sundström, E., Luthman, J., Goldstein, M., and Jonsson, G. (1988). Time course of MPTP-induced degeneration of the nigrostriatal dopamine system in C57 BL/6 mice. Brain Res. Bull. *21*, 257–263.

56. Fornai, F., Chen, K., Giorgi, F.S., Gesi, M., Alessandri, M.G., and Shih, J.C. (1999). Striatal dopamine metabolism in monoamine oxidase B-deficient mice: a brain dialysis study. J. Neurochem. *73*, 2434–2440.

57. Dickson, D.W., Braak, H., Duda, J.E., Duyckaerts, C., Gasser, T., Halliday, G.M., Hardy, J., Leverenz, J.B., Del Tredici, K., Wszolek, Z.K., and Litvan, I. (2009). Neuropathological assessment of Parkinson's disease: refining the diagnostic criteria. Lancet Neurol. *8*, 1150–1157.

58. Olanow, C.W., Rascol, O., Hauser, R., Feigin, P.D., Jankovic, J., Lang, A., Langston, W., Melamed, E., Poewe, W., Stocchi, F., and Tolosa, E.; ADAGIO Study Investigators (2009). A double-blind, delayed-start trial of rasagiline in Parkinson's disease. N. Engl. J. Med. *361*, 1268–1278.

59. Pålhagen, S., Heinonen, E., Hägglund, J., Kaugesaar, T., Mäki-Ikola, O., and Palm, R.; Swedish Parkinson Study Group (2006). Selegiline slows the progression of the symptoms of Parkinson disease. Neurology *66*, 1200–1206.

60. Binde, C.D., Tvete, I.F., Gåsemyr, J., Natvig, B., and Klemp, M. (2018). A multiple treatment comparison meta-analysis of monoamine oxidase type B inhibitors for Parkinson's disease. Br. J. Clin. Pharmacol. *84*, 1917–1927.

61. Edmondson, D.E. (2014). Hydrogen peroxide produced by mitochondrial monoamine oxidase catalysis: biological implications. Curr. Pharm. Des. *20*, 155–160.

62. Mallajosyula, J.K., Kaur, D., Chinta, S.J., Rajagopalan, S., Rane, A., Nicholls, D.G., Di Monte, D.A., Macarthur, H., and Andersen, J.K. (2008). MAO-B elevation in mouse brain astrocytes results in Parkinson's pathology. PLoS ONE *3*, e1616.

63. Liddelow, S.A., Guttenplan, K.A., Clarke, L.E., Bennett, F.C., Bohlen, C.J., Schirmer, L., Bennett, M.L., Münch, A.E., Chung, W.S., Peterson, T.C., et al. (2017). Neurotoxic reactive astrocytes are induced by activated microglia. Nature *541*, 481–487.

64. Yoon, H.H., Min, J., Hwang, E., Lee, C.J., Suh, J.K., Hwang, O., and Jeon, S.R. (2016). Optogenetic inhibition of the subthalamic nucleus reduces levodopa-induced dyskinesias in a rat model of Parkinson's disease. Stereotact. Funct. Neurosurg. *94*, 41–53.

65. Paxinos, G., and Watson, C. (1998). The Rat Brain in Stereotaxic Coordinates (Academic Press).

66. Son, H.J., Lee, J.A., Shin, N., Choi, J.H., Seo, J.W., Chi, D.Y., Lee, C.S., Kim, E.M., Choe, H., and Hwang, O. (2012). A novel compound PTIQ protects the nigral dopaminergic neurones in an animal model of Parkinson's disease induced by MPTP. Br. J. Pharmacol. *165*, 2213–2227.

67. Lee, K.H., Lujan, J.L., Trevathan, J.K., Ross, E.K., Bartoletta, J.J., Park, H.O., Paek, S.B., Nicolai, E.N., Lee, J.H., Min, H.K., et al. (2017). WINCS Harmoni: closed-loop dynamic neurochemical control of therapeutic interventions. Sci. Rep. *7*, 46675.

68. Oh, Y., Park, C., Kim, D.H., Shin, H., Kang, Y.M., DeWaele, M., Lee, J., Min, H.K., Blaha, C.D., Bennet, K.E., et al. (2016). Monitoring in vivo changes in tonic extracellular dopamine level by charge-balancing multiple waveform fast-scan cyclic voltammetry. Anal. Chem. *88*, 10962–10970.

69. Simola, N., Morelli, M., and Carta, A.R. (2007). The 6-hydroxydopamine model of Parkinson's disease. Neurotox. Res. *11*, 151–167.

STAR★METHODS

KEY RESOURCES TABLE

REAGENT or RESOURCE	SOURCE	IDENTIFIER
Antibodies		
Rabbit anti-TH	Pel-freez	Cat# p40101-0; RRID: AB_461064
Rabbit anti-TH	Abcam	Cat# ab112; RRID: AB_297840
Mouse anti-TH	Sigma aldrich	Cat# T2928; RRID: AB_477569
Rabbit anti-DDC	Abcam	Cat# ab3905; RRID: AB_304145
Chicken anti-GFAP	Millipore	Cat# ab5541; RRID: AB_177521
Guinea pig anti-GABA	Millipore	Cat# ab175; RRID: AB_91011
Rabbit anti-GABA	Millipore	Cat# ab131; RRID: AB_2278931
Rabbit anti-Gat1	Millipore	Cat# ab1570; RRID: AB_90790
Rabbit anti-Gat3	Millipore	Cat# ab1574; RRID: AB_90779
Rabbit anti-ABAT	Abcam	Cat# 3359-1; RRID: AB_10641072
Rabbit anti-GAD65/67	Millipore	Cat# AB1511; RRID: AB_90715
Mouse anti-GAD67	Merck	Cat# MAB5406B; RRID: AB_2278725
Rabbit anti-Maob	Sigma aldrich	Cat# HPA002328; RRID: AB_1854062
Mouse anti-putrescine	Dr. Fujiwara	N/A
Rabbit anti-PAT	Novus	Cat# NBP1-81931; RRID: AB_11009423
Mouse anti-a-synuclein	Abcam	Cat# ab1903; RRID: AB_302665
Mouse anti-GAD67	Millipore	Cat# MAB5406B; RRID: AB_2278725
DAPI	Pierce	Cat# D1306; RRID: AB_2629482
Alexa 488 goat anti-rabbit	Thermo Fisher Scientific	Cat# A-11034; RRID: AB_2576217
Alexa-594 goat anti-rabbit	Thermo Fisher Scientific	Cat# A-11012, RRID: AB_2534079
Alexa 488 goat anti-chicken	Thermo Fisher Scientific	Cat# A-11039, RRID: AB_2534096
Alexa-594 goat anti- guinea pig	Thermo Fisher Scientific	Cat# A-11076, RRID: AB_2534120
Alexa-647 goat anti-rabbit	Thermo Fisher Scientific	Cat# A21244; RRID: AB_2535812
Bacterial and Virus Strains		
AAV-A53T	KIST virus facility	N/A
AAV-eGFP	KIST virus facility	N/A
AAV-hSynapsin1-NpHR-YFP	KIST virus facility	N/A
AAV-hSynapsin1-ChR2-YFP	KIST virus facility	N/A
lentivirus (pSicoR-PATshRNA-mCherry)	KIST virus facility	N/A
Biological Samples		
Human brain samples	Boston University Alzheimer's Disease Center (BUADC)	N/A
Chemicals, Peptides, and Recombinant Proteins		
MPTP(1-methyl-4-phenyl-1,2,3,6-tetrahydropyridine)-HCl	Sigma aldrich	Cat# M0896; CAS: 23007-85-4
6-OHDA(6-hydroxydopamine)	Sigma aldrich	Cat# H4381; CAS: 28094-15-7
R(-)-deprenyl hydrochloride, selegiline	Sigma aldrich	Cat# M003; CAS: 14611-52-0
safinamide	This paper	N/A
Kainic acid	Sigma aldrich	Cat# K0250; CAS: 58002-62-3
Putrescine hydrochloride	Sigma aldrich	Cat# P5780; CAS: 333-93-7
D-AP5	Tocris	Cat# 0106; CAS: 79055-68-8
CNQX	Tocris	Cat# 0190; CAS: 115066-14-3
(-)-Bicuculline methobromide	Tocris	Cat# 0109; CAS: 73604-30-5
Apomorphine	Sigma aldrich	Cat# A4393; CAS: 41372-20-7
Fura-2AM	Invitrogen	Cat# F-1201; CAS: 108964-32-5

(*Continued on next page*)

Continued

REAGENT or RESOURCE	SOURCE	IDENTIFIER
Critical Commercial Assays		
Amplex Red Monoamine Oxidase Assay Kit	Thermo Fisher Scientific	Cat#: A12214
Experimental Models: Cell Lines		
Human: HEK293T cells	Korean Cell Line Bank (Seoul National University)	RRID: CVCL_0045
Experimental Models: Organisms/Strains		
Mouse: C57BL6/J	The Jackson Laboratory	Cat# JAX:000664
Mouse: B6.B6D2-Tg(Th-EGFP)21-31Koba	RIKEN BioResource Center	Cat# RBRC02095
Mouse: B6;129S-*Maob*^{tm1Shih}/J	The Jackson Laboratory	Cat# JAX:014133
Mouse: C57BL/6-Tg(Gfap-rtTA,tetO-MAOB,-lacZ)1Jkan/J	The Jackson Laboratory	Cat# JAX:017955
Mouse: ICR	The Jackson Laboratory	Cat# JAX:009122
Rat: Wistar rat	Orient Bio, Korea	N/A
Oligonucleotides		
Primer: Mouse Pat qRT-F; AGT GTC GCT GCA GTA TG	This paper	N/A
Primer: Mouse Pat qRT-R; CCT CTG CTG CCA TTT TTA GC	This paper	N/A
Primer: Mouse Gapdh qRT-F; ACC CAG AAG ACT GTG GAT GG	This paper	N/A
Primer: Mouse Gapdh qRT-R; CAC ATT GGG GGT AGG AAC AC	This paper	N/A
Primer: Human Gfap qRT-F; CTT TGC CAG CTA CAT CGA GA	This paper	N/A
Primer: Human Gfap qRT-R; ATT GTC CCT CTC AAC CTC CA	This paper	N/A
Primer: Human Mao-b qRT-F; CCC ACC TGT ATG GAA TCC A	This paper	N/A
Primer: Human Mao-b qRT-R; CAG TGA CAC ACA GGT TCA CA	This paper	N/A
Primer: Human Gapdh qRT-F; ACA GCC GCA TCT TCT TGT GCA GTG	This paper	N/A
Primer: Human Gapdh qRT-R; GGC CTT GAC TGT GCC GTT GAA TTT	This paper	N/A
shRNA targeting sequence: CTA CCA AGA AGT GCA TAC TGC	This paper	N/A
Recombinant DNA		
pSicoR-PATshRNA-mCherry	This paper	N/A
Software and Algorithms		
GraphPad Prism 7	GraphPad software	https://www.megasoftware.net/home; RRID: SCR_005375
NIS-Elements	Nikon	https://www.nikonmetrology.com/en-gb/product/nis-elements-microscope-imaging-software
ImageJ program	NIH	https://imagej.nih.gov/ij/download.html
Minianalysis	Synaptosoft	http://www.synaptosoft.com/MiniAnalysis/
NeuroExplorer software	Nex Technologies	https://www.neuroexplorer.com/downloadspage/

LEAD CONTACT AND MATERIALS AVAILABILITY

Further information and requests for resources and reagents should be directed to and will be fulfilled by the Lead Contact, C. Justin Lee (cjl@ibs.re.kr). This study did not generate new unique reagents.

EXPERIMENTAL MODEL AND SUBJECT DETAILS

Animals

All mice and rats were kept in a temperature- and humidity-controlled environment with a 12-h light-dark cycle (lights on at 9 a.m.) and had free access to food and water. All animal care and handling was performed according to the directives of the Animal Care and Use Committee of the Institutional Animal Care and Use Committee of KIST (Seoul, Korea) and Asan Institute for Life Sciences (Seoul, Korea). For MPTP PD model, male C57BL/6 mice (10-week-old when injecting MPTP), for 6-OHDA PD model and AAV-hSyn-NpHR-YFP injection, male Wistar rats (250∼300 g at the beginning of the experiment), for A53T mouse PD model, male MAO-B KO and WT littermate mice (9–10-week-old when injecting AAV-A53T virus; 129 strain), for A53T rat PD model and MPP+ PD model, male Wistar rats (8–10-week-old when injecting AAV-A53T virus or MPP+) were used. For kainic acid injection, 8-week-old male ICR mice were used. For putrescine injection, PAT shRNA injection, 9-week old male C57BL/6 mice were used. For slice electrophysiological experiments, TH-EGFP transgenic mice were used. 190 mice, 36 rats were subjected to behavioral tests. All experiments were done with age-matched controls. Different sets of animals were used for each experiment.

For investigating the effects of MAO-B inhibitors, R-(–)-deprenyl hydrochloride (selegiline; Sigma aldrich, MO, USA), safinamide (10 mg/kg/day) were applied by oral injection (3-day pre- and post-treatment for MPTP mice model and 15-day treatment for 6-OHDA rat model). In terms of 30-day treatment for MPTP model, the mice were provided with 50 mL of water (control), selegiline and safinamide solution (66.67 mg/L in water) *ad libitum*. The solution was changed every two days for preventing from decaying of effects of the compounds. Dose was calculated as 5–10 mg/kg/day.

MPTP mouse model

All MPTP experiments used the acute regimen consisting of four times of intraperitoneal injection of MPTP-HCl (M0896, Sigma Aldrich, 2 mg/mL in saline, 20 mg/kg for one injection) in a day with 2 h intervals. MPTP use and safety precautions were as described [37].

6-OHDA rat model

6-OHDA model was prepared as previously described [64]. Under general anesthesia, all rats received unilateral injections of 8 μg 6-OHDA (Sigma aldrich) in 4 μL of saline with 0.1% ascorbic acid into the right medial forebrain bundle (AP −2.2 mm, L +1.5 mm relative to the bregma, and V −8.0 mm from the dura) [65], with the tooth bar set at +4.5 mm. To confirm if 6-OHDA model is successfully prepared, the apomorphine (0.25 mg/kg, s.c. administration, Sigma aldrich)-induced rotation test was performed with automated rotometer (Panlab, Barcelona, Spain). Inclusion criteria was above 6 rpm.

α-synuclein mouse or rat model

Stereotaxic injections of AAV-A53T virus or AAV-eGFP virus (packaged by KIST virus facility), as a control, (right mouse SN: AP −3.2, ML −1.3, DV 4.0; right rat SN; AP −5.3, ML −2.3, DV −7.6 relative to the bregma; 0.2 μL/min, total 2 μL) [65] was performed under general anesthesia induced by avertin (mouse) or chloral hydrate (rat) [33]. AAV viruses used here are driven by CMV promoter.

MPP+ rat model

Under general anesthesia using chloral hydrate, stereotaxic injections of MPP+ (right MFB; A/P −3.6, M/L −2.0, D/V −7.5 relative to the bregma; 7.4 g MPP+ in 2 μL PBS, Sigma) [48, 65] was performed.

Human brain samples

Neuropathological processing of normal, mild, and severe (advanced) PD human brain samples followed the procedures previously established for the Boston University Alzheimer's Disease Center (BUADC). Institutional Review Board approval for ethical permission was obtained through the BUADC. Next of kin provided informed consent for participation and brain donation. The study was performed in accordance with principles of human subject protection in the Declaration of Helsinki.

Normal brains included four females and 3 males with no significant lewy pathology, a median age of 78.2 and an age range of 63 - 99 years. PD human brains were from two females and nine males with a median age of 87.9 and an age range of 70 - 107 years. To categorically define cases with severe versus mild PD, TH immunocytochemistry was performed on midbrain sections from 7 pathologically confirmed control patients and 11 patients with Lewy body PD as described below in detailed methods. TH positive neurons were counted by tracing of neurons in the SNpc. TH counts in the normal SN ranged from 98-107 cells/mm^2 (Figure 7D). TH counts in the SN of the PD cases ranged from 9-81 cells/mm^2 (Figure 7D). An arbitrary cutoff of 40 cells/mm^2 was made to categorically define cases with severe versus mild loss of TH neurons (n = 5 and 6 for mild and severe, respectively).

METHOD DETAILS

Optogenetics

Virus preparation and injection for optogenetics

The AAV vector plasmid, pAAV2-hSynapsin1-NpHR-YFP or pAAV2-hSynapsin1-ChR2-YFP, was constructed by removing the CMV promoter from pAAV2-CMV (Stratagene, La Jolla, CA) and inserting the hSynapsin1 promoter and NpHR-YFP sequence (plasmid

#26775, Addgene) or ChR2-YFP sequence (plasmid #26969 Addgene). pAAV-RC plasmid harbors the AAV rep and cap genes encoding the replication and virus capsid structure protein, respectively. The pHelper plasmid contains the essential subset of adenovirus genes, VA, E2A, and E4 necessary for AAV production in HEK293 cells. For AAV2/2 production, three AAV plasmids (10 μg of each plasmid) were co-transfected into HEK293 cells using a polyethylenimine (PEI) transfection kit (Polyplus, Illkirch-Graffenstaden, France).

The minimum number of viral particles was 1.0×10^{10}/mL, which is a concentrated virus package. Viral injections were performed under general anesthesia induced by intraperitoneal injection of a mixture of 35 mg/kg zoletil (Virbac S.A, Carros, France) and 5 mg/kg rompun (Bayer, Leverkusen, Germany). All rats (n = 12) were received injections of 2.0 μL AAV-hSynapsin1-NpHR-YFP or pAAV2-hSynapsin1-ChR2-YFP targeted at the right SNpc (coordinates: AP = −5.6 mm, ML = +2.0 mm relative to the bregma, and DV = −7.5 mm from the dura) (*49*). The virus was delivered at a rate of 0.2 μL/min using a 33-gauge Hamilton syringe and an automated microsyringe pump (Harvard Apparatus, Holliston, MA). After injection, the needle was kept in place for 5 min to prevent the solution from flowing backward and was then retracted over a subsequent 5 min.

Experimental design of optogenetic inhibition

Two weeks after viral injection of AAV-hSyn-NpHR-YFP (packaged by KIST virus facility) into right SNpc, the optic fiber was implanted into the ipsilateral SNpc.

Experimental design of optogenetic activation

Six rats received unilateral injections of AAV-A53T and AAV-hSyn-ChR2-YFP (packaged by KIST virus facility) into right SNpc. Seven 6-OHDA model rats received the AAV-hSyn-ChR2-YFP injection into right SNpc. Twenty days after viral injection, the optic fiber was implanted into the ipsilateral SNpc. Two 6-OHDA model rats with inappropriate infection of virus that had little or no response to stepping test were excluded.

Optic fiber implantation for optogenetics

Optic fibers (200 μm core, 245 μm outer diameter, numerical aperture (NA) 0.53, RM3 type, and flat tip; Doric lenses; Québec, Canada) were cut to the length of 8.3 mm to optimize SN depth. Two weeks after injection of AAV, the animals were positioned in a stereotactic frame under general anesthesia. After scalp incision, four burr holes were drilled to fix screws around the insertion site of the optic fiber. The optic fiber was implanted using a stereotactic cannula holder into the SNpc at the same site of AAV injection. The optic fiber was firmly fixed with surrounding screws using dental cement (Vertex; Zeist, Nederland).

Light stimulation

For light stimulations, the optic fiber was connected to the fiber-optic rotary joint and LED fiber-optic light-source (Doric lenses) that produces amber light (590 nm; output power with fiber 200 μm: 0.663 mW) or blue (470 nm) light (output power with fiber 200 μm: 1.160 mW). The output power was measured using a power meter (Newport 1936-R with a photodetector 918D-SL-0D3R). For optogenetic activation, the light source was modulated by function generator (HYSEN, Seoul, Korea) with 5-Hz trains of light pulses lasting 6 ms of width. The 24 h of light illumination were performed in freely moving animals.

Electrophysiology for optogenetics

Whole-cell patch-clamp for NpHR- or ChR2-positive dopaminergic neurons in SNpc was performed as described in tonic GABA recording, with alteration of intrapipette solution as follows: 140 K-gluconate, 10 HEPES, 7 NaCl, pH adjusted to 7.2 with KOH (280–290 mOsmol). For validating the functionality of NpHR, under current clamp mode, 200 pA of current was injected for one second to induce action potential firing. After confirmation of action potential firing, amber light (590 nm) was shed through light guide cable whose end is placed next to the cell, during another current injection. For validating the functionality of ChR2, Under current clamp mode, spontaneous firing was recorded. During recording spontaneous firing, blue light (470 nm) was shed through light guide cable whose end is placed next to the cell. The light source was modulated by Digidata 1440A using pCLAMP 10.2 software.

Behavioral tests

Vertical grid test

The vertical grid test was performed as described in the previous study [53]. Briefly, a mouse was gently placed inside the apparatus at 3 cm from the top, facing upward, and was allowed to turn around and climb down after 2-day habituation.

Hindlimb test

Hindlimb test was performed six days after MPTP injection, as previously described [66]. Mice were scored on a scale of 0 to 4 in hindlimb movement of the joint or limb. A score of 1 was deducted for each abnormal hindlimb movement.

Rotarod test

Rotarod test for MPTP model was performed as previously described [66]. Briefly, prior to MPTP administration, a 2-day habituation was allowed to mice, and the actual test was performed at a fixed speed of 30 rpm on the 6th day after MPTP administration. For A53T model, we performed rotarod test at 15 rpm after 21 days from AAV-A53T virus injection, with slight modification of a previously described protocol [51]. The only difference in the protocols is the duration of a single training session which reduced from 120 s to 60 s.

Stepping test

The stepping test was performed as previously described with slight modifications [52]. Briefly, both hindlimbs and one forelimb were firmly fixed in the two hands of the experimenter, and the rostral part of the rat was lowered onto a treadmill moving at rate of 18 cm/s. The rat's body remained stationary while the unilateral forelimb was allowed to spontaneously touch the moving treadmill track for 10 s. All of the experiment sessions were video-recorded to allow the number of adjusted steps taken in the backward direction to be

counted. The number of adjusting steps was averaged across the four trials in each session. The stepping test before the 24 h of light illumination (Pre-test) and under the light illumination after the 24 h of light illumination (Light-test). For optogenetic inhibition, stepping test was additionally performed on 1 day or 5 days after the 24 h of light illumination (Post-test).

DAB staining for TH and DDC

The 30-μm-thick coronal sections for striatum and SNpc were immunostained with a DAB staining kit (TL-060-QHD, Thermo, MA, USA). The sections were incubated in Hydrogen Peroxide Block (TA-060-HP, Thermo) for 10 min, washed in PBS 3 times, incubated for 5 min in Ultravision Block (TA-060-UB, Thermo) and washed in PBS 3 times again. Then the samples were immunostained with a mixture of primary antibodies in a blocking solution (0.3% Triton-X, 2% ready-to-use donkey serum (GTX30972, Genetex, CA, USA) in 0.1 M PBS) at 4°C on a shaker overnight. After washing in PBS 3 times, sections were incubated in Primary Antibody Amplifier Quanto (TA-060-QPB, Thermo) for 5 min, and washed in PBS again. The sections were incubated in HRP Polymer Quanto for 1 h and washed 4 times in PBS. DAB+ chromogen and DAB+ substrate buffer (K3468, Dako, Denmark) were mixed in 1:10 ratio and the sections were dipped in the mixture for 30 s and then washed. Finally, sections were mounted with mounting solution and dried. A series of bright field images were obtained with an Olympus microscope.

For human samples, the human brain sections were deparaffinized and dehydrated through a series of ethanol. The sections were incubated in 3% Hydrogen Peroxide for 10 min, washed in TBS 3 times and incubated for 1 h in Blocking solution (5% BSA, 0.3% Triton X-100 in 0.02 M TBS). Then the sections were immunostained for primary antibodies at 4°C on a shaker overnight. After washing in TBS 2 times, sections were incubated with biotinylated secondary antibodies (1:200, Jackson Lab) for 1 h and subsequently with ABC reagents (PK-6100, Vector Labs) for 1 h. Antibody complexes were visualized by using DAB peroxidase substrate kit (SK-4105, Vector Labs). After DAB, sections were mounted with mounting solution and dried. A series of bright field images were obtained with an Olympus microscope.

Slice immunostaining for confocal microscopy

Sections were first incubated for 1 h in a blocking solution (0.3% Triton-X, 2% normal serum in 0.1 M PBS) and then immunostained with a mixture of primary antibodies in a blocking solution at 4°C. After extensive washing, sections were incubated with corresponding fluorescent secondary antibodies for 2 h and then washed with PBS 3 times. If needed, DAPI (1:3,000, Pierce) staining was performed. Finally, sections were mounted with fluorescent mounting medium (S3023, Dako) and dried. A series of fluorescent images were obtained with an A1 Nikon confocal microscope, and Z stack images in 2-μm steps were processed for further analysis using or NIS-Elements (Nikon, Japan) software and ImageJ program (NIH, MD, USA). Any alterations in brightness or contrast were equally applied to the entire image set. Specificity of primary antibody and immunoreaction was confirmed by omitting primary antibodies or changing fluorescent probes of the secondary antibodies.

For human samples, the tissue slides were incubated for 1 h in a blocking solution (5% BSA, 0.3% Triton X-100 in 0.02 M TBS) and then immunostained with a mixture of primary antibodies in a blocking solution at 4°C on a shaker overnight. After washing in TBS 2 times, sections were incubated for 1 h with corresponding fluorescent secondary antibodies and then washed with TBS 3 times. The nuclei were counter stained with DAPI, and fluorescence signals were visualized using an A1 Nikon confocal microscope.

PI staining *in vivo*

To detect dead cells, PI was administrated as described in the previous study [27]. Briefly, 4 mg/kg of PI (Sigma Aldrich) was injected into the tail vein of mice. After 5 h, the mice were sacrificed, and 30-μm-thick sections from the obtained brain tissues were prepared for confocal microscopy imaging. As a positive control, seizure mouse models induced by kainic acid (20 mg/kg, i.p., Sigma Aldrich) were used.

Virus and putrescine injection

Lentivirus containing PAT shRNA (packaged by KIST virus facility) was injected into bilateral SNpc (AP = −3.2, ML = ± 1.3 relative to the bregma, DV = −4.0 from dura; 0.2 μL/min, total 2 μL). For putrescine injection, cannulation was performed 5 days prior to injection. Putrescine hydrochloride (Sigma Aldrich) was dissolved in saline and injected into bilateral SNpc (0.2 μL/min, total 0.5 μL) through cannula without anesthesia.

In vivo fast-scan cyclic voltammetry

Electrochemical electrode fabrication

The carbon-fiber microelectrode (CFM) design was fabricated by isolating and inserting a single carbon fiber (AS4, d = 7 μm; Hexel, Dublin, CA) into a silica tubing (20μM ID, 90μM OD, 10μM coat with polyimide; Polymicro Technologies, Phoenix, AZ). The connection between the carbon fiber and the silica tubing was covered with polyamic acid (Sigma-Aldrich, St. Louis, MO) and heated to 200°C to polymerize the polyamic acid into a polyimide film. The silica tubing was then attached to a nitinol (Nitinol #1, an alloy of nickel and titanium; Fort Wayne Metals, IN) extension wire with a silver-based conductive paste1. The carbon fiber attached nitinol wire was insulated with polyimide tubing (0.0089"ID, 0.0134"OD, 0.00225" WT; Vention Medical, Salem, NH) except the carbon fiber sensing part. The exposed carbon fiber was trimmed under a dissecting microscope to a length of approximately 50-100 μm. Teflon-coated silver wire (A-M systems, Inc., Sequim, WA) was prepared as an Ag/AgCl reference electrode and chlorinating the exposed tip in saline with a 9 V dry cell battery.

In vivo *electrochemical measurement protocol*

The mice were anesthetized with an injection of urethane (1.6 g/kg, i.p.) and stabilized in a commercially available stereotaxic frame (David Kopf Instruments, Tujunga, CA) for the surgery. A longitudinal incision was made on the skin to expose the skull and three burr holes (0.5-1.0 mm diameter) were made in the skull of each mouse for the implantation of a CFM, a bipolar electrical stimulating electrode (Plastic One, MS303/2, Roanoke, VA, USA) and an Ag/AgCl reference electrode. The reference electrode was positioned superficially in cortical tissue contralateral to the CFM and stimulating electrode. Electrode coordinates were referenced by a mouse brain atlas based on flat-skull position using bregma and dura as reference points. The CFM was placed in the right hemisphere in the striatum (AP +0.8 mm; ML +1.2 mm; DV −2.2 to −3.2 mm), and the stimulating electrode was inserted ipsilaterally in the SNpc (AP −3.2; ML +1.3; DV −3.9 to −4.1). WINCS Harmoni was used to perform FSCV and electrical stimulation to identify dopamine releasing site. A train of bipolar pulses (2 ms pulse width, 300 μA, 60 Hz) using WINCS Harmoni electrometer was delivered for 3 s to identify dopamine releasing sites in the striatum. FSCV signal was synchronized with electrical stimulation in order to interleave intervals of stimulation during FSCV scans [67]. Thus, electrical stimulation was not applied when the FSCV pulses (about 10ms) were delivered. A scan rate of 400 V/s and holding potential of −0.4 V versus Ag/AgCl were used between scans, the switching potential was 1.3V, and scans were repeated every 100 ms to match the repetition time (10 Hz) of the proposed waveform. The CFM and the electrical stimulating electrode were gradually adjusted until a robust phasic DA signal was detected at the CFM using FSCV. To quantify the FSCV DA voltammogram for each electrode, a flow-injection analysis system was used, which consisted of a syringe pump (Harvard Apparatus, Holliston, MA) that directed a buffer solution through a Teflon tube to a 6-port injection valve (Rheodyne, Rohnert Park, CA), was used for *in vitro* measurements. The injection valve was controlled by a 12 V DC solenoid and was used to transport the analyte from an injection loop to an electrochemical flow cell at a rate of 2 mL/min. A CFM was placed in a flowing stream of buffer, and analyte was injected as a bolus to calibrate each electrode with known concentrations of DA. DA was dissolved in distilled water at a stock concentration of 1 mM diluted with TRIS buffer (15 mM tris(hydroxymethyl)aminomethane, 3.25 mM KCl, 140 mM NaCl, 1.2 mM CaCl2, 1.25 mM NaH2PO4, 1.2 mM MgCl2, and 2.0 mM Na2SO4, with the pH adjusted to 7.4) and preserved in 0.1 M perchloric [68]. From this stock solution, dilutions were made in TRIS buffer for desired final concentrations before starting the flow injection experiments. 1 μM DA flow cell response was used for the electrode calibration.

In vivo microdialysis

Mice were anesthetized by 2% avertin i.p injection and placed on a stereotaxic apparatus (model 900, David Kopf, CA, USA) to implant a guide cannula (CMA7, CAM Microdialysis, Sweden) into the SNpc (AP = 3.2, ML = 1.3, VM = 3.6 from the bregma). After at least 7 d after surgery, microdialysis probes were inserted into the brain and experiments were carried out in freely moving animals. Dialysis probes (CMA7, CAM Microdialysis; 0.24 mm outer diameter, with 6000 Da M.W. cutoff) would be located 1 mm from guide cannula. Mouse was placed in a Perspex cage and the inlet cannula connected by polythene tubing (Portex Ltd., UK) to a 1 mL syringe, mounted on a CMA/102 microinjection pump (CMA Microdialysis) containing artificial cerebrospinal fluid (aCSF, composition in mM: 147 NaCl, 2.7 KCl, 1.2 CaCl2, 0.85 MgCl2) of CMA perfusion fluid for CNS. Probes were perfused with aCSF at a constant flow-rate of 2 μL/min. Samples were automatically collected every 20 min using CMA 470 refrigerated microfraction collector and stored at −70°C until analyzed.

L-glutamate and γ-butyric acid measurement

1 mg/mL stock solutions of GABA/glutamate standards were prepared in HPLC grade water, aliquoted out and stored at −20°C. Working solutions (1 μg/mL and 5 μg/mL for glutamate; 100 ng/mL and 500 ng/mL for GABA) were prepared daily by dilutions of those stock solutions, aliquoted out and stored at 4°C until derivatization and analysis. Briefly, the derivatization was performed by mixing 100 μL sample or standards solutions, 20 μL of daily prepared methanolic OPA (5 mg/mL), 75 μL borate buffer (pH 9.9) and 5 μL MPA. The resulting solution was vortexed and analyzed after 1-min at room temperature. The HPLC system consisted of a Waters chromatograph (Waters, MA, USA) with a 200 μL loop (Rheodyne 7725-I, CA, USA) and a fluorescence detector (FLD-Waters spectrofluorometric detector waters 2475, MA, USA), coupled to an LC-10 AD PUMP. The system was equipped with a 3 μm particle size (150 mm × 4.6 mm, ID) C18 analytical column (Hibar-Futigsanle RT) and a pre-packed column (RT 250-4 E. Merck, Darmstadt E.R., Germany). An integrator (Empower 2) was used to analyze the chromatographic data. The mobile phase consisted of 0.05 M sodium acetate, tetrahydrofuran and methanol (50:1:49, v/v) adjusted to pH 4.0. The mobile phase was filtered through Millipore 0.45 μm durapore membrane filters and vacuum degassed prior to use. Chromatographic analyses were performed at 25 ± 2°C. Compounds were eluted isocratically over a 9 min runtime at a flow rate of 1 mL/min. The fluorescent detector was set at an excitation wavelength of 337 nm and an emission wavelength of 454 nm, low sensitivity and range GABA/glutamate were identified by their characteristic retention times as determined by standard injections. Sample peak areas were measured through the integrator system and compared with the calibration curve standard in order to quantify the amino acids concentrations.

Quantitative real-time PCR

Quantitative RT-PCR (qRT-PCR) was carried out using SYBR Green PCR Master Mix as described previously [27]. In brief, reactions were performed in duplicates in a total volume of 10 mL containing 10 pM primer, 4 mL cDNA, and 5 mL power SYBR Green PCR Master Mix (Applied Biosystems). The mRNA level of PAT was normalized to that of Gapdh mRNA. Fold-induction was calculated using the 2–DDCT method.

For human samples, RNA was isolated using NucleoSpin Total RNA isolation kit (Macherey-Nagel), and cDNA was generated by Maxime RT PreMix Oligo dT primer kit (Intron biotechnology). By performing qRT-PCR on the cDNA samples using an ABI Stepone 2.1 (Applied Biosystems), the mRNA levels of GFAP and MAO-B were measured. Human GAPDH was used as an endogenous control to standardize the amount of RNA in each reaction.

Measurements of MAO-B enzyme activity

MAO-B activity in tissue of 6-OHDA model was determined using a commercially available kit (A12214; Thermo Fisher Scientific), following the manufacturer's protocol. Lysates were prepared from each region of 6-OHDA model by centrifuging at 16,000rpm after homogenization with RIPA lysis buffer with phosphatase and protease inhibitor cocktail (Roche, Switzerland). Protein concentration in the supernatant was determined using a Bradford-based assay (Bio-Rad Laboratories, Hercules, CA, USA), and samples were diluted to 500 μg per 2 mL total volume with reaction buffer. Samples were pre-incubated for 30 min at room temperature with the specific MAO-B inhibitor, pargyline hydrochloride (1 μM). After incubation, samples were added to individual wells of a 96-well microplate. The fluorimetric assay was initiated by adding 100 μL of a reaction mixture containing Amplex Red reagent (400 μM), horseradish peroxidase (HRP; 2 U/mL) and benzylamine (2 mM), a specific substrate of MAO-B. Plates were incubated for 30 min at room temperature, protected from light, and fluorescence was measured at excitation and emission wavelengths of 550 nm and 590 nm, respectively, using a microplate fluorometer (Life Sciences, Manchester, UK). H2O2 (10 μM) was used as a positive control, and reaction buffer alone was used as a negative control.

Sniffer patch with acutely dissociated astrocytes

Sniffer patch was performed as described with a slight modification [27]. The quickly excised brain was submerged in ice-cold cutting solution that contained (in mM): 250 sucrose, 26 NaHCO3, 10 d-(+)-glucose, 4 MgCl2, 3 myo-inositol, 2.5 KCl, 2 sodium pyruvate, 1.25 NaH2PO4, 0.5 ascorbic acid, 0.1 CaCl2 and 1 kynurenic acid, pH 7.4. All solution was gassed with 95% O2 – 5% CO2. The brain regions containing SNpc were coronally sliced in 300 μm-thickness using a vibrating microtome (VT1000S, Leica, Germany). The SNpc region was then isolated and astrocytes were acutely dissociated and prepared as previously detailed [27]. HEK293T cells, originated from Korean Cell Line Bank (Seoul National University, Korea) and mycoplasma free, expressing $GABA_CR$ and EGFP were added onto the cover glass with acutely dissociated cells. According to a previous report, astrocytes can be identified morphologically. To determine whether GFP-expressing HEK293T cells express GABACR, 100 μM GABA was bath-applied to induce GABACR-mediated full current. To block Ca^{2+}-activated Cl– channel-mediated GABA release, NPPB was pretreated for 5 min. The whole procedures of sniffer patch was performed as previously detailed [27].

Tonic GABA recording

$GABA_A$-receptor–mediated current in SNpc was measured as previously described for hippocampal tonic GABA recording [27]. Prior to recording, 300 μm-thick SNpc-containing slices from freshly prepared brains were incubated at room temperature for at least 1 h in aCSF solution: 126 NaCl, 24 $NaHCO_3$, 1 NaH_2PO_4, 0.5 ascorbic acid, 2.5 KCl, 2.5 CaCl2, 2 $MgCl_2$, and 10 D-(+)-glucose, pH 7.4. For recording, slices were transferred to a recording chamber that was continuously perfused with aCSF solution (flow rate = 2 mL/min). The slice chamber was mounted on the stage of an upright Olympus microscope and visualized with a 60 × water immersion objective (NA = 0.90) with infrared differential interference contrast optics and a CCD camera and by using Imaging Workbench software (Indec BioSystems, CA, USA). Whole-cell recordings were performed from DA cell somata located in SNpc. The holding potential was −70 mV. Pipette resistance was typically 6–8 MΩ and the pipette was filled with an internal solution: 135 CsCl, 4 NaCl, 0.5 $CaCl_2$, 10 HEPES, 5 EGTA, 2 Mg-ATP, 0.5 Na_2-GTP, 10 QX-314, pH adjusted to 7.2 with CsOH (278–285 mOsmol). Before measuring tonic current, baseline current was stabilized with D-AP5 (50 μM) and CNQX (20 μM). Electrical signals were digitized and sampled at 50-ms intervals with Digidata 1440A and Multiclamp 700B amplifier (Molecular Devices) using pCLAMP 10.2 software. Data were filtered at 2 kHz. The amplitude of tonic GABA current was measured by the baseline shift after bicuculline (50 μM) administration using the Clampfit program. For investigating the change of extrasynaptic GABA receptors, tonic current was measured by the baseline shift between before and after bicuculline (50 μM) administration under saturating concentration of GABA (5 μM) treatment (*52*). Frequency and amplitude of spontaneous inhibitory post-synaptic currents (sIPSCs) before bicuculline administration was detected and measured by Minianalysis (Synaptosoft, NJ, USA).

Cell-attached patch-clamp

For obtaining of the innate firing rate of DA neurons, cell-attached patch clamp was performed. Slices were transferred to a small-volume recording chamber that was located on fixed-stage, upright microscope (Olympus). Experiments were performed at room temperature in oxygenated aCSF. Following previous studies, the SNpc was defined as the region between the medial leminiscus dorsally and the SNpr ventrally [69]. DA neurons identified with large cell bodies and with dendritic processes running in a mediolateral manner and were distinguished according to their distinct electrophysiological property which is a 3-4 Hz firing pattern, prominent voltage-sag during hyperpolarizing current injection and confirmed with TH-EGFP mice. Pipette resistance was 3-6 MΩ containing with recording solution. For recording in cell-attached mode, the cell was maintained at holding potential that was applied to achieve 0 pA injected current. Recording started after stable baseline formatted, about 5 min. For selegiline group, brain slices from MPTP model was pre-incubated for 1 h with selegiline (100 nM).

In vivo unit recording

The animals were anesthetized with 2% avertin (20 μg/g, i.p.) or urethane (1 g/kg, i.p.) and mounted on a stereotaxic frame (David Kopf Instruments, CA, USA). After incision and removing of the skin from the surface on the skull, a hole is drilled for insertion of 40 μm-thick single shank type silicon neural probe into SNpc (mouse, AP = −3.2, ML = 1.3 from bregma, DV = −3.5 ~4.5 from the dura; rat, AP = −5.6, ML = 2.3 from Bregma, DV = −6.2 ~7.5 from the dura). Unit spikes from 16-channel of silicon neural probe were acquired at a sampling rate of 32 kHz using the digital recording system (Digital Lynx 4SX, Neuralynx, MT, USA). Individual spike data were recorded simultaneously by applying two different bandpass filter parameters: 0.6 ~6000 Hz and 300 ~6000 Hz, respectively. The shank of silicon neural probe consists of 19 μm x 19 μm iridium microelectrodes which are evenly spaced with a center to center spacing of approximately 20 μm.

Single-unit spike sorting was performed using Offline Sorter (Plexon, TX, USA). All waveforms were plotted in a principal component space and clusters consisting of similar waveforms were defined manually. A cluster of waveforms distinct from other clusters in principal component space and showing a clear refractory period (> 1 ms) was considered to be generating from a single neuron. To examine basal firing properties, the mean firing rate from separated clusters were calculated over the recording period (3 min) with NeuroExplorer software (Nex Technologies, MA, USA). After completion of experiments, the probe insertion was confirmed histologically. Mice were transcardially perfused with 0.9% saline followed by 4% PFA. Brains were removed and kept in PFA overnight for post-fixation. Coronal sections (80 μm) were obtained using vibratome (VT1200S, Leica, Germany) and examined under light microscope. In many cases a fluorescent dye (DiI, Molecular Probes, MA, USA) was applied to the one side of electrode for visualizing the electrode track.

QUANTIFICATION AND STATISTICAL ANALYSIS

Image quantification

Confocal microscopic images were analyzed using the ImageJ program (NIH). For defining TH (or DDC)-negative or -positive cells, after measuring the intensity of TH and DDC, we considered the cells with the TH (or DDC) intensity of under 10 as TH (or DDC)-negative cells. For measurement of GFAP+ area, the image was transformed into binary and then the white pixels were measured. To obtain GABA intensity of the GABA+ area which is colocalized with GFAP, we first made GFAP+ image binary and made GABA+ image into 8 bit. Next we multiplied the GFAP+ binary image with 8-bit GABA+ image. Then we could get the image of grayscaled GABA pixels only in the GFAP+ area. From this image, we measured the intensity of GABA+ pixels in the whole image, which is the y axis scale, the GABA intensity in GFAP+ area indicating GABA contents in GFAP+ astrocytes. For analyzing GABA intensity in an astrocyte, the images were converted into binary and every GFAP+ astrocytes were picked as region of interest (ROI). Then the mean intensity value of GABA in every ROI was measured. For densitometric analysis of the striatum area with TH staining, coronal sections of striatum were observed under a bright field microscope (Olympus, PA, USA) using 10 x magnification. The optical density of the TH-stained striatum was determined at an equivalent frame range, with optical density in the corpus callosum used as a reference. Four-to-five mice per group were sacrificed, and three-to-five slices per mouse were stained and analyzed for quantification of TH. The sizes of DDC+ cells were measured after the images were converted into binary.

To quantify the cell number in human SNpc tissues, tracing of neurons in the SNpc was performed by superimposing photo images using Photoshop software. Neuronal clusters were divided into four major groups based on the histologic anatomy such as ventrolateral tier (VL), ventromedial tier (VM), dorsal tier (D), and pars lateralis (L). For statistical analysis, at least five sections per group were counted. The number of GFAP, GABA, DDC, and neuromelanin$^+$ neurons in the ventrolateral SNpc was presented as cells/mm^2.

Stereology

An unbiased stereological estimation of the total number of TH$^+$ neurons in the SN area of A53T models and MPTP models was performed using the optical fractionator method using Stereo Investigator 11 (11.01.2 64-bit, MBF Bioscience). The counted sections covered the entire SN, from the rostral tip of the SNpc to the caudal end of the SNpr (substantia nigra pars reticulate). An unbiased counting frame of known area (47.87 × 36.19 μm = 1733 μm^2) was placed randomly on the first counting area and systematically moved through all counting areas until the entire delineated area was sampled. Counting was performed using a low-magnification objective lens (× 10). The total number of neurons was estimated according to the optical fractionator formula.

Statistical analyses

Statistical analyses were performed using Prism 7 (GraphPad Software). Differences between two different groups were analyzed with the two-tailed Student's unpaired t test. For assessment of change of a group by a certain intervention, the significance of data was assessed by the two-tailed Student's paired t test. For comparison of multiple groups, one-way analysis of variance (ANOVA) with Tukey's or Dunnett's multiple comparison test, or two-way ANOVA with Bonferroni's multiple comparison test was assessed. Data from multiple independent experiments was assumed to be normal variance. Data was assumed to be normally distributed. $p < 0.05$ was considered to indicate statistical significance throughout the study. The significance level is represented as asterisks (*$p < 0.05$, **$p < 0.01$, ***$p < 0.001$; ns, not significant). Detailed statistical analysis contents are described in Table S2. Unless otherwise specified, all data are presented as mean ± SEM. No statistical method was used to predetermine sample size. Sample sizes were determined empirically based on our previous experiences or the review of similar experiments in literatures. The numbers of animals used are described in the corresponding figure legends or on each graph. All experiments were done with at

least three biological replicates. Experimental groups were balanced in terms of animal age, sex and weight. Animals were genotyped before experiments, and they were all caged together and treated in the same way. Prior to administration of neurotoxins, animals were randomly and evenly allocated to each experimental group. However, investigators were not blinded to group allocation during experiments or to outcome assessments. No data points were excluded, except only for stepping behavior with optogenetic activation of 6-OHDA rats; 2 mice showing inappropriate infection of ChR2-carrying virus were excluded from the analysis.

DATA AND CODE AVAILABILITY

No large-scale datasets or new code were generated in this study.